Tectonics

RESEARCH ARTICLE
10.1029/2021TC007009

Assessing the Internal Uppermost Crustal Structure of the Central Pyrenees by Gravity-Constrained Cross Sections

Ruth Soto[1], Pilar Clariana[1], Conxi Ayala[2,3], Carmen Rey-Moral[4], Antonio M. Casas-Sainz[5], Teresa Román-Berdiel[5], Aina Margalef[6], Félix Rubio[4], Belén Oliva-Urcia[7], Emilio L. Pueyo[1], Juliana Martín-León[4], and Elisabet Beamud[8]

[1]Instituto Geológico y Minero de España, CSIC, Unidad de Zaragoza, Zaragoza, Spain, [2]Instituto Geológico y Minero de España, CSIC, Madrid, Spain, [3]Currently visiting researcher at Geosciencies Barcelona (Geo3Bcn CSIC), Barcelona, Spain, [4]Instituto Geológico y Minero de España, CSIC, Madrid, Spain, [5]Geotransfer (IUCA), Universidad de Zaragoza, Zaragoza, Spain, [6]Andorra Recerca + Innovació, Institut d'Estudis Andorrans (IEA), Sant Julià de Lòria, Andorra, Principat d'Andorra, [7]Universidad de Zaragoza, Zaragoza, Spain, [8]Unitat de Paleomagnetisme (CCiTUB-CSIC), Geosciences Barcelona (Geo3Bcn CSIC), Barcelona, Spain

Key Points:

- Gravity, petrophysical and geological data are integrated to constrain the geometry of the upper crust of the Central Pyrenees
- Bouguer and residual anomalies and six serial gravity-constrained cross sections of the study area are obtained
- Gravity variations respond to changes in the volume of Triassic evaporites, the geometry of the igneous bodies, and lateral structural variations

Correspondence to:
R. Soto,
r.soto@igme.es

Citation:
Soto, R., Clariana, P., Ayala, C., Rey-Moral, C., Casas-Sainz, A. M., Román-Berdiel, T., et al. (2022). Assessing the internal uppermost crustal structure of the Central Pyrenees by gravity-constrained cross sections. *Tectonics*, *41*, e2021TC007009. https://doi.org/10.1029/2021TC007009

Received 29 JUL 2021
Accepted 27 JUL 2022

Author Contributions:
Conceptualization: Ruth Soto, Pilar Clariana, Conxi Ayala
Formal analysis: Ruth Soto, Pilar Clariana, Conxi Ayala, Carmen Rey-Moral, Félix Rubio
Funding acquisition: Conxi Ayala
Investigation: Ruth Soto, Pilar Clariana, Conxi Ayala, Carmen Rey-Moral, Antonio M. Casas-Sainz, Teresa Román-Berdiel, Aina Margalef, Félix Rubio, Belén Oliva-Urcia, Emilio L. Pueyo
Methodology: Ruth Soto, Pilar Clariana, Conxi Ayala, Félix Rubio
Project Administration: Conxi Ayala
Resources: Conxi Ayala
Software: Conxi Ayala, Carmen Rey-Moral, Félix Rubio, Juliana Martín-León
Supervision: Ruth Soto

Abstract The Pyrenees constitutes an exceptional example of an Alpine orogenic belt characterized by basement thrust sheets involving Paleozoic rocks and Mesozoic and Cenozoic cover units detached on the Triassic evaporites, the main décollement level. This work is located in the Central Pyrenees, where gravity data help to better constrain the internal architecture of the upper crust of the southern half of the Axial Zone and the northern part of the South Pyrenean Zone, a key area to understand the orogenic evolution of the chain. Previous and new gravity, petrophysical and geological data have been used to obtain the Bouguer and residual anomaly maps of the study area and six serial gravity-constrained cross sections perpendicular to the main structural trend. The residual anomaly map shows a good correlation between basement units involved in thrust sheets of the study area and gravity highs whereas negative anomalies are interpreted to correspond with Mesozoic/Cenozoic basins, Triassic evaporites, Late Variscan igneous bodies, and Ordovician gneisses. The six gravity-constrained cross sections highlight strong along-strike variations on the gravity signal due to lateral differences of the superficial and subsurface occurrence of Triassic evaporites, different geometry at depth of the Late Variscan igneous bodies outcropping in the study area, and geometric lateral variations of the basement thrust sheets and their relationship with the Mesozoic-Cenozoic units.

1. Introduction

The integration of geophysical modeling to classical structural studies constitutes a powerful approach to inferring the Earth's crust architecture (e.g., Calcagno et al., 2008; Crombez et al., 2020; Godin & Harris, 2014; Jessel, 2001). Focusing on the upper crust, the characterization of the crustal-basement structure and its relationships with the overlying sedimentary cover has deserved much attention during the last decades due to its implications for heat-flow prediction and hydrocarbon system modeling (e.g., Forster & Smith, 1989; Ten Brink et al., 1993). Obtaining an accurate interpretation of the upper crustal structure is not easy, especially in areas where data arising from wells and/or seismic sections are absent or scarce. Gravity data, due to their relative low acquisition cost, wide availability, and well-established processing and interpretation techniques, constitute a valid and widespread geophysical method used in the upper crust to study basement geometries (e.g., Ayala et al., 2019; Goleby et al., 1989; Izquierdo-Llavall et al., 2019), assess the internal structure and thickness of allochthonous complexes (Martínez Catalán et al., 2012), delineate the distribution and geometry of evaporitic bodies and/or evaporitic detachment levels (e.g., Ali et al., 2014; Calvín et al., 2018; Santolaria et al., 2016, 2020; Sarsar-Naouali et al., 2011) and/or study geometry at depth of granitic bodies (e.g., Aranguren et al., 2003; Terrinha et al., 2018; Vigneresse & Clemens, 2000).

In the last decades, considerable progress has been made in understanding the crustal and lithospheric structure of the Pyrenees based on several geophysical methods; wide-angle reflection/refraction profiles (Daignières et al., 1981; Gallart et al., 1981), vertical incidence reflection profiles (e.g., ECORS-Pyrenees Team, 1988; Muñoz, 1992), analyzing seismic and teleseismic data (e.g., Chevrot et al., 2018; Díaz et al., 2012; Wang et al., 2016), magnetotelluric data (e.g., Campanyà et al., 2011, 2012; Ledo et al., 2000), magnetic anomalies (e.g., Canva et al., 2020), seismic tomography (e.g., Chevrot et al., 2014), heat flow (e.g., Fernàndez et al., 1990)

Validation: Ruth Soto, Conxi Ayala, Carmen Rey-Moral, Félix Rubio
Visualization: Ruth Soto, Juliana Martín-León
Writing – original draft: Ruth Soto

and gravimetric data (Casas et al., 1997; Pedrera et al., 2017; Rivero et al., 2002; Torné et al., 1989, 2015; Vacher & Souriau, 2001). As numerous works demonstrate, the crustal deep structure of the Pyrenees constitutes a first-order element controlling the evolution of the Pyrenees and also its uppermost structure (e.g., Beaumont et al., 2000; Soto et al., 2006; Jammes et al., 2009; Saspiturry et al., 2019; Muñoz, 2019 and references therein). A rapid glance at the crustal structure of the Pyrenees can be done by looking at its Bouguer anomaly map (e.g., Ayala et al., 2016; Casas et al., 1997; Torné et al., 1989) (Figure 1). It shows from North to South a high-amplitude positive-negative-positive anomaly pattern across the WNW-ESE Pyrenean direction. The large negative anomaly reaching c. −100 mGal coincides with the core of the chain and is caused by the thick Pyrenean crustal roots (Torné et al., 2015). In the Northern Pyrenees, strong positive anomalies have been related to uplifted dense bodies (from the either lower crust or mantle) (e.g., Casas et al., 1997; Pedrera et al., 2017; Vacher & Souriau, 2001). To the North and South, a higher but laterally variable −60 to 5 mGal gravity response corresponds to the sedimentary filling at its foreland basins, the Aquitanian and Ebro basins (Figure 1). The area studied in this work lies on the long-wavelength large negative anomaly at the core of the chain (up to 400 km). This area also shows, at a shorter wavelength (c. 2 km), different relative gravity maxima and minima whose detailed analysis adding a dense gravity prospecting constitute one of the main targets of this work (Figure 1).

Interpretations deduced from gravity data are non-unique and different models can fit the same observations (e.g., Blakely, 1996; Crombez et al., 2020; LaFehr & Nabighian, 2013). Decreasing the range of possible solutions represents one of the major challenges when modeling subsurface geology (e.g., Crombez et al., 2020; Saltus & Blakely, 2011). The relatively well-known geology with exceptional outcrops and availability of geophysical data make the Central Pyrenees the ideal candidate for attempting to better understand their upper crustal structure and analyze the gravity response of their different geological crustal bodies. This approach can be applied to other orogenic areas with less subsurface information where gravity data are available.

2. Geological Setting

The Pyrenees are a WNW-ESE asymmetric mountain range with a mainly southwards vergence, developed from the Late Cretaceous to the Early Miocene (e.g., Muñoz, 1992). It resulted from the convergence between the Iberian and European plates which was accommodated by underthrusting of the Iberian lithosphere underneath Europe and thrusting and stacking of the upper crust (e.g., Choukroune and ECORS team, 1989; Roest & Srivastava, 1991; Robenbaum et al., 2002). The present-day crustal architecture of the Pyrenees results from a complex evolution influenced by several factors such as the re-activation of previous Variscan structures and/or inversion of inherited Mesozoic extensional basins (e.g., Bond & McClay, 1995; Martínez-Peña & Casas-Sainz, 2003; Muñoz, 1992; Vergés et al., 1995), weakness of the inherited Variscan crust and the lithospheric thermal state inherited from Early Mesozoic rifting stages (e.g., Clerc & Lagabrielle, 2014; Jammes et al., 2014; Jammes & Huismans, 2012), and the distribution and position of mechanically weak horizons (e.g., Beaumont et al., 2000; Muñoz, 1992). Regarding the last factor, in the Pyrenees three main different weak horizons have been recognized to control its evolution: (a) a mid-crustal weak zone decoupling the Iberian crust in the Central Pyrenees (e.g., Beaumont et al., 2000; Muñoz, 1992), (b) the Silurian shales acting as an effective décollement in Variscan and Alpine basement thrust sheets (e.g., Casas et al., 2019; Cochelin et al., 2017; García-Sansegundo, 1990; García-Sansegundo et al., 2011; Marcén et al., 2018; Matte, 1969), and (c) the Mid-Upper Triassic evaporites which exert a major control on the tectonic style of the North and South Pyrenean Zones (e.g., Ford & Vergés, 2021; Muñoz, 1992).

The overall geometry and structural architecture of the mountain range have already been established based on numerous geological and geophysical data obtained during several decades. The regional cross sections constructed in different sectors of the mountain belt point to an along-strike variability of the basement and sedimentary cover structure (e.g., Casas et al., 1997; Casas and Faccenna, 2001; Chevrot et al., 2018; Espurt et al., 2019; Martínez-Peña & Casas-Sainz, 2003; Muñoz, 1992; Teixell, 1998; Vergés et al., 1995). Across the central part of the chain, 167 km of shortening have been estimated (Muñoz, 1992). Geophysical data coming from a series of receiver-functions profiles crossing the Pyrenees also show an along-strike variability on its deep crustal architecture (Chevrot et al., 2015, 2018).

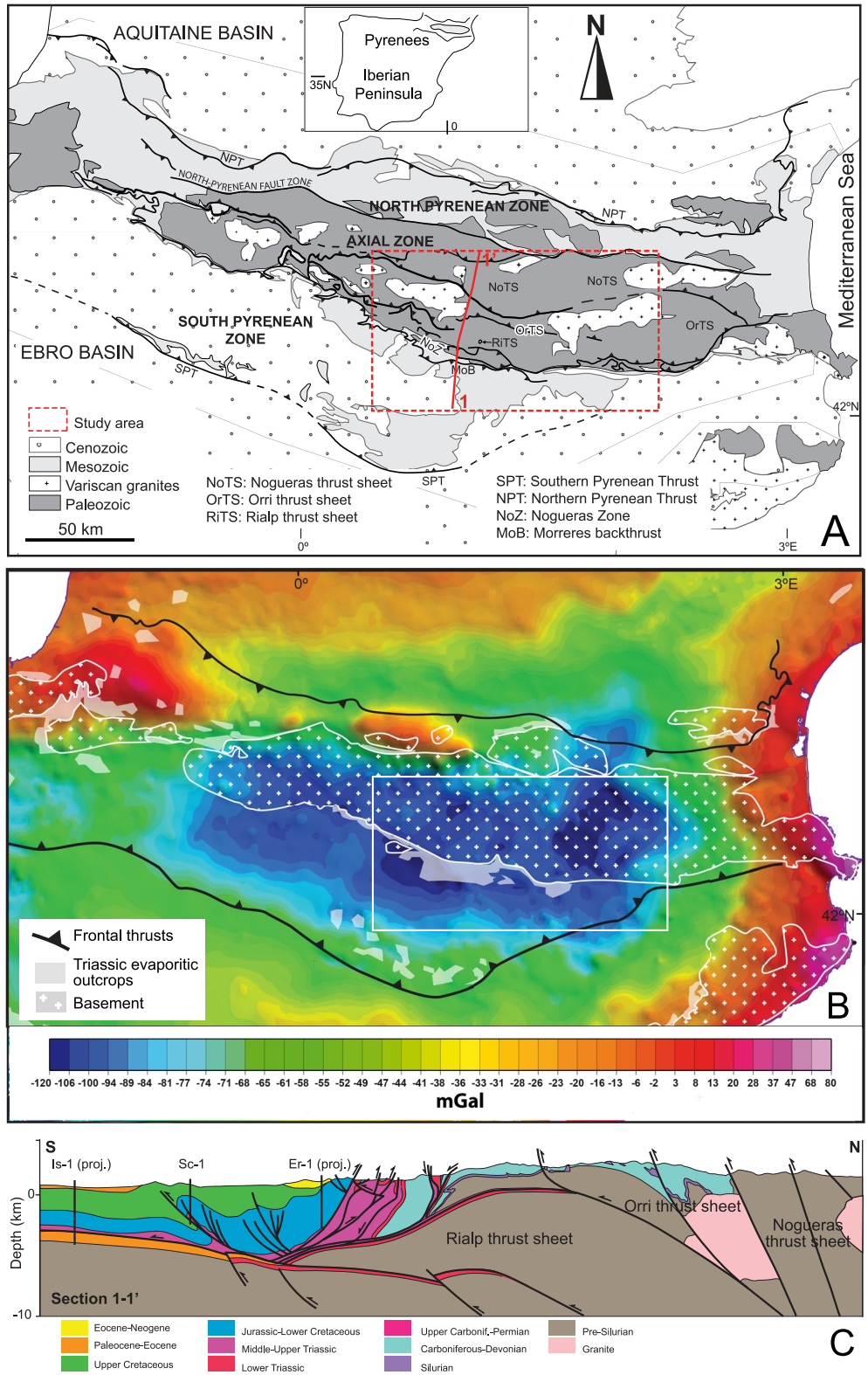

Figure 1. (a) Tectonic sketch map of the Pyrenees, showing the main basement and cover units and the study area (in dashed red rectangle). (b) Bouguer anomaly map of the Pyrenees showing the study area (modified from Ayala et al., 2016). The location of the Paleozoic basement and Triassic evaporitic rocks is also shown. (c) Geological cross section along the ECORS profile (modified from Muñoz et al. [2018]). Location on Figure 1A.

2.1. Structural Overview

The study area is located in the central sector of the Central Pyrenees and comprises the southern half of the Axial Zone and the northernmost part of the South Pyrenean Zone (Figures 1 and 2a).

In the Axial Zone of the Central Pyrenees, Alpine deformation in the Paleozoic basement was accommodated by several south-verging thrust sheets varying along-strike in number and distribution (e.g., Espurt et al., 2019; García-Sansegundo, 1992; García-Senz et al., 2020; Izquierdo-Llavall et al., 2018; Labaume et al., 2016; Martínez-Peña & Casas-Sainz, 2003; Muñoz, 1992; Parish, 1984; Teixell, 1996; Teixell et al., 2018; Williams, 1985). In the western part of the study area four basement thrust sheets can be differentiated, which from top to bottom are (e.g., Muñoz et al., 2018): Nogueras, Orri, Rialp, and Ribagorza (not outcropping) (Figure 2b). Toward the east, only the first three basement units, Nogueras, Orri, and Rialp thrust sheets, are differentiated (Muñoz, 1992; Vergés, 1993; see Figure 1c). These basement thrust units form an antiformal stack whose sequential pattern is characterized by underthrusting of the lower and younger basement-involved thrust sheets (e.g., Muñoz, 1992). Consequently, the structures of the uppermost unit (the Nogueras thrust sheet) have been tilted in the southern leading edge of the antiformal stack showing downward facing structures and involving upper Paleozoic rocks and Permian to Lower Triassic red beds (Figure 2; Nogueras Zone; e.g., Seguret [1972]). Toward the west and east of the study area, these basement thrust sheets show a smaller vertical overlap and downward facing structures are not found (Martínez-Peña & Casas-Sainz, 2003; Saura & Teixell, 2006; Teixell, 1996; Vergés, 1993).

South of the Axial Zone, the Mesozoic-Cenozoic cover was decoupled from the basement along the Triassic evaporites and deformed in a thin-skinned style following a forward propagating thrust sequence from the Late Cretaceous to the Oligocene (e.g., Muñoz, 1992; Seguret, 1972; Vergés, 1993). The study area includes the Bóixols thrust sheet, which continues to the west into the Cotiella thrust sheet (e.g., García-Senz, 2002) and to the Upper Pedraforca thrust sheet to the east (e.g., Muñoz et al., 2018), a small portion of the Montsec thrust unit and its eastern continuation, the Middle Pedraforca thrust sheet (Muñoz et al., 2018) and the Lower Pedraforca thrust sheet (Figure 2b). The Bóixols and Montsec thrust sheets belong to a thrust salient developed as a progressive arc due both to a thrust displacement gradient and changes in the mechanical stratigraphy (Muñoz et al., 2013; Sussman et al., 2004). The Ebro foreland basin appears in the southeastern portion of the study area (Figure 2). These sediments continue in the foot-wall, below the allochthonous Pyrenean thrust sheets, as shown by seismic and well data (e.g., Muñoz et al., 2018; Vergés, 1993). Located in the Axial Zone of the study area, the Cerdanya basin (see Figure 2b) is filled with Neogene rocks related to an ENE-WSW oriented half-graben (e.g., Cabrera et al., 1988).

2.2. Stratigraphic Units

The Axial Zone is formed, in the study area, by sedimentary, igneous, and high-, medium- and low-grade metamorphic rocks of Cambrian to Carboniferous age deformed during the Variscan Orogeny (Middle-Late Carboniferous; Capellà, 1991; Clariana, 2015; Denèle, 2007; García-Sansegundo, 1992; Margalef, 2015) unconformably overlain by Stephanian, Permian, and Triassic rocks (Zwart, 1979) (Figure 2a). The oldest outcropping sedimentary record corresponds to Cambrian and Ordovician siliciclastic rocks with some intercalations of limestones and microconglomerates. Above, the Silurian black shales constitute an important detachment level (e.g., García-Sansegundo, 1990; Matte, 1969), as mentioned previously, below the Devonian slates and limestones (Zwart, 1979). The Carboniferous series, older than the Stephanian succession, mainly consist of siliciclastic rocks (Devolvé, 1987). The Late Carboniferous (Stephanian)-Permian succession is mainly formed by andesitic lava flows and pyroclastic units with some interbedded coal beds and red sandstones, shales, and microconglomerates (e.g., Gisbert, 1983; Mey et al., 1968). This succession is unconformably covered by the Triassic sediments, which show the typical Germanic facies (Calvet et al., 2004): Lower Triassic red beds (Buntsandstein facies), Middle Triassic dolostones and limestones (Muschelkalk facies) and Upper Triassic evaporites and shales (Keuper facies). Tholeiitic subvolcanic rocks (i.e., dolerites) are relatively common within the Upper Triassic series (Lago et al., 2000).

Intrusive rocks are represented by syn-to late-Variscan granitoids (Late Carboniferous-Early Permian in age) (Figure 2), which intrude the pre-Late Carboniferous succession (e.g., Evans, 1993; López-Sánchez et al., 2019; Solé et al., 1997) (Figure 2) and produced local contact metamorphism (e.g., Autran et al., 1970). The metamorphic rocks showing the highest metamorphic grade are located in the northeastern sector of the study area where

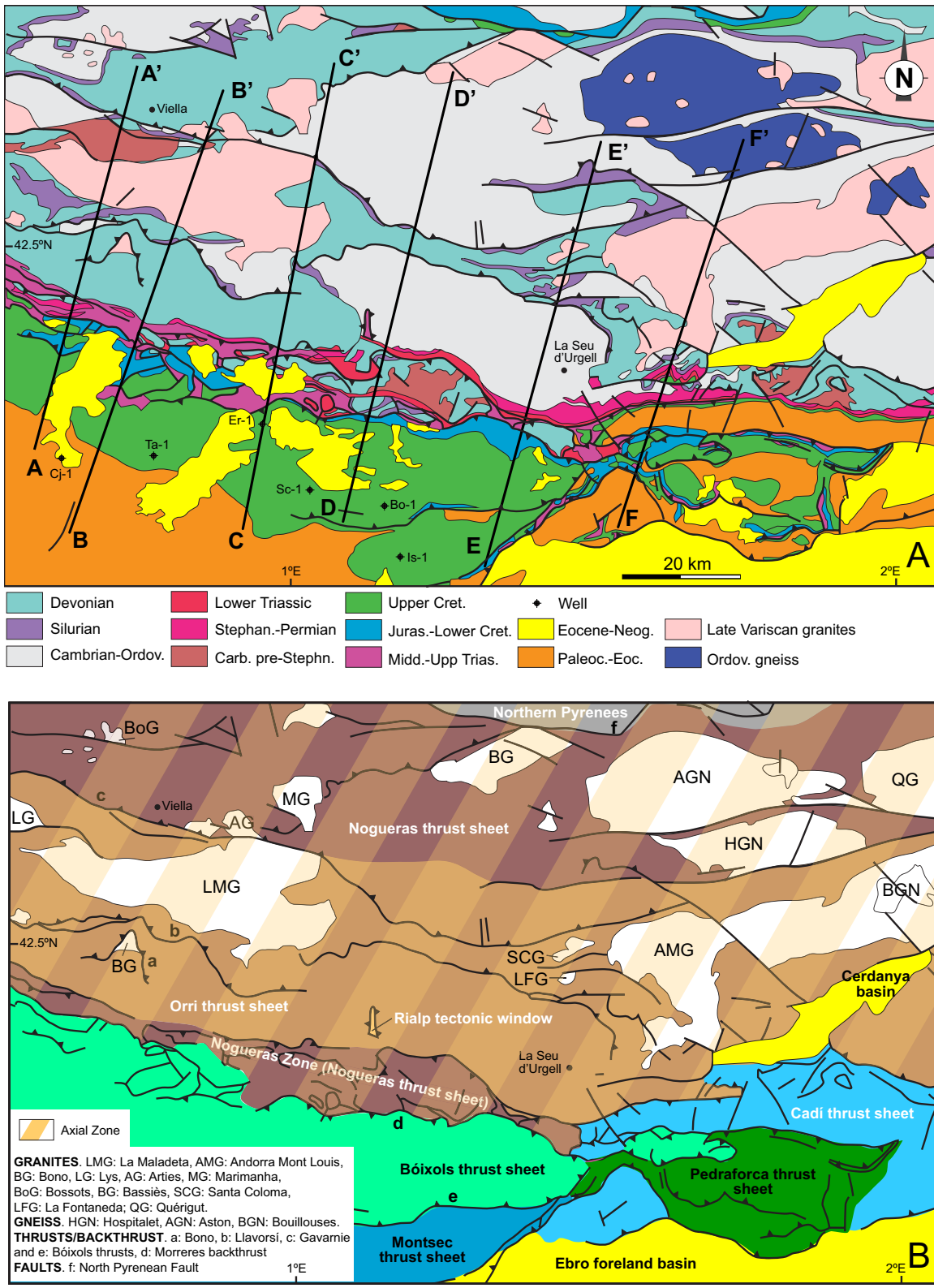

Figure 2. (a) Geological map with the location of the modeled sections A-A' to F-F' and Tamurcia-1, Cajigar-1, Erinyà-1, San Corneli-1, Bóixols-1 and Isona-1 wells (Comiols-1 well is located outside the study area) (well data; see Lanaja [1987]; Mencos et al. [2015]). (b) Sketch showing the main structural units of the study area.

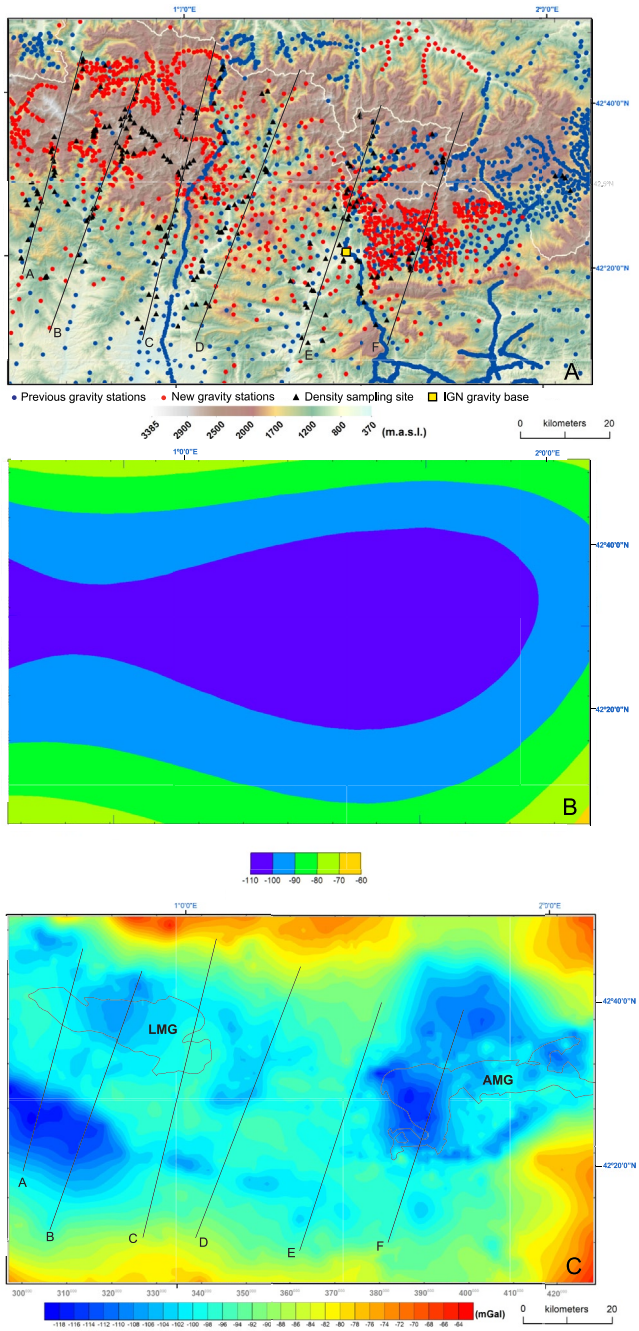

Figure 3. (a) Relief map of the study area showing the previous and new acquired gravity stations considered in this work and the density sampling sites. In yellow square IGN (Instituto Geográfico Nacional) gravity base of La Seu d'Urgell. The color scale refers to the elevation in meters above sea level. (b) Regional anomaly map of the study area. (c) Bouguer anomaly map of the study area. Contour interval is 2.50 mGal. The location of the modeled sections A-A' to F-F' is shown. LMG = La Maladeta granite and AMG = Andorra Mont-Louis granite.

three Ordovician gneiss domes crop out (Figure 2). These gneiss domes are characterized by a core of ortho-to paragneisses (Denèle et al., 2014) and an envelope of Cambrian and Ordovician metasedimentary rocks affected by a high temperature-low pressure metamorphic gradient from the biotite zone to the garnet, andalusite-staurolite-cordierite, staurolite and sillimanite zones (Alías, 1995; Clariana, 2015; Guitard et al., 1996).

The Mesozoic-Cenozoic cover in the study area consists of thick sequences of Jurassic and Lower Cretaceous, mainly marine limestones and marls, deposited in relation to previous extensional basins (e.g., García-Senz, 2002). The Upper Cretaceous series is characterized by a succession of limestones, calcarenites, and marls (Simó, 2004). The Paleocene-Eocene series mainly consists of limestones, sandstones, and marls of marine origin, together with non-marine sandstones and conglomerates; whereas the youngest deposits considered in the study area are Oligocene and Neogene continental units, mainly conglomerates and sandstones (e.g., Barnolas & Gil-Peña, 2001; Martínez et al., 1988; Puigdefàbregas & Souquet, 1986).

3. Gravity Data Acquisition and Processing

Gravity data used in this study is a compilation of public gravity datasets (ICC, 1987; BRGM, 2009; IGC-ICC-ICTJA-CSIC, 2012), previous works (Ayala et al., 2020; Casas et al., 1987, 1997; Rivero Marginedas, 1994; Torné et al., 1989) and new gravity surveys. In total, 3,590 gravity stations have been used in an area of ~10,000 km^2, 2,449 previous and 1,141 new stations. Gravity station distribution is not homogeneous showing a higher number of measurements on La Maladeta and Andorra-Mont Louis granites only along accessible tracks (Figure 3). Elevation and spatial positioning of the new gravity data were obtained using a differential GNSS instrument (Triumph from Javad). New gravity measurements were taken with a Scintrex CG5 (63% stations), a Lacoste & Romberg G582 (25% stations) and a Scintrex CG6 (12% stations). Data were linked to La Seu d'Urgell base that belongs to the IGN's Fundamental Network directly linked to the IGSN71 network and other stations that coincide with the ones of the IGN REDNAP high precision leveling network. Gravity measurements were corrected for effects caused by instrumental drift and tides to obtain the observed gravity.

A complete Bouguer anomaly was recalculated for the entire dataset using the Geodetic Reference System GRS80 (Moritz, 1980), and a density of reduction of 2.67 g/cm^3 (Figure 3). The terrain correction was applied up to 167 km using the Oasis Montaj module based on Kane (1962) and Nagy (1969). We use a combined 5 m DTM from Spain, France, and Andorra that was regridded to 20 × 20 m as a local grid considering a radius of 2 km, and a combined grid from the SRTM database (e.g., Farr et al., 2007) and bathymetry data from GEBCO database (Sandwell et al., 2002) regridded to 100 × 100 m as regional grid considering a radius of 167 km.

Bouguer anomalies result from the combination of sources at different depths related to density contrasts; the deep-seated geological bodies or huge shallow sedimentary basins generate the long-wavelength components of the anomaly and the small and near-surface geological bodies originate the short-wavelength components.

In order to investigate gravity anomalies related to the uppermost crust, a regional-residual separation was obtained. The selected regional gravity anomaly (assumed as the contribution of deeper sources) consists of a third order polynomial surface (Figure 3b). The regional anomaly was chosen after doing a careful analysis of

different regional anomalies (i.e., isostatic calculation based on the Airy hypothesis, assuming different polynomial degrees and using a different type of filters) and estimating the radially averaged power spectrum. The regional anomaly was subtracted from the Bouguer anomaly (Figure 3c) in order to obtain the residual Bouguer anomaly (Figure 4), which in our work we assume allows modeling down to ~10,000 m depth, where the structures that are the target of this study are located. Additionally, vertical and horizontal gradients of the residual anomaly were calculated (Figures 5a–b5c). This enhances the edges between geological bodies of different densities and defines particular structural alignments that can be associated with faults or lithological contacts at depth. Taking into account the main structural trend of the Pyrenees, a N110 E direction, we also calculated the horizontal gradients both in the N110 E and N200 E (i.e., parallel and perpendicular to the Pyrenean trend respectively) directions (Figures 5b and 5c).

4. Bouguer and Residual Gravity Anomaly Maps

In the entire study area, the Bouguer anomaly shows negative values between approximately −120 and −67.5 mGal (Figure 3c). The central part of the study area is characterized by a long-wavelength elongated relative minimum associated with the crustal Pyrenean root (see Torné et al., 1989) which follows a roughly N110 E direction. The orientation of this long minimum is parallel to the southern limit of the Axial Zone and most Alpine structures (Figures 1 and 3). Superimposed to this minimum, several relative maxima, and minima of medium and short wavelengths with variable amplitudes can be observed (Figure 3c). The most prominent of these relative minima are (a) a N110 E oriented relative minimum located to the South of the southern limit of the Axial Zone (i.e., located on the Nogueras Zone and Bóixols thrust sheet; see Figures 1 and 2) which reaches more than −115 mGal and amplitude of ~25 mGal and (b) a minimum formed by two rounded gravity lows aligned in an NNE direction reaching more than −110 mGal and an amplitude of 15–20 mGal located inside the Axial Zone and coinciding at the South with the western part of the Andorra-Mont Louis granite (Figures 2 and 3). The first of these relative minima can be continued to the East following a roughly N110 E orientation and along a total of ~125 km before it is closed to the East by a N-S positive gradient. The gravity response of the La Maladeta granite coincides with a relative minimum showing variations in the amplitude of only 5 to 10 mGal, smaller than that shown by the Andorra-Mont Louis granite (Figures 2 and 3).

The residual gravity anomalies range from −18 to 18 mGal (Figure 4). The residual gravity anomaly map shows two areas with a different residual anomaly pattern; the Axial Zone and the South Pyrenean Zone (Figure 4). Both areas are separated by a Pyrenean-oriented limit, which roughly coincides with the southern termination of the Axial Zone with values around 0 mGal. In the Axial Zone, the residual anomaly pattern is complex (Figure 4a). Gravity lows labeled as 1 and 2 in Figure 4a show a Pyrenean-oriented trend. Gravity low 1 reaches −18 mGal and coincides at the surface with the outcrops of the Arties and Bossost granites (Figure 4b). Gravity low 2 shows lesser amplitude than the previous one (~−4 mGal) and coincides with the Aston and Hospitalet gneisses (Figure 4b). To the East, the gravity minima 3 and 4 coincide with the Andorra-Mont Louis granite and the Neogene Cerdanya basin, respectively (Figure 4). The gravity maximum 5 displays a noteworthy NNE-SSW in the central sector of the studied Axial Zone (Figure 4). In the South Pyrenean Zone, the large Pyrenean-oriented gravity minimum labeled as 6 coincides with the Bòixols and Pedraforca thrust sheets and partly with the Nogueras Zone (Figure 4). It shows its lowest gravity values (−18 mGal) in a large minimum labeled as 7 in Figure 4a. Positive gravity values surround the gravity low six except at its SW corner (Figure 4).

The vertical gradient of the residual anomaly map enhances the negative gravity anomaly of the Late Carboniferous-Early Permian granites, Ordovician gneisses, and the Cerdanya Cenozoic basin in the Axial Zone and the Triassic evaporites at depth in the South Pyrenean Zone (Figure 5a). Whereas the horizontal gradient map along the N200 E direction enhances the negative gravity anomaly 6, which coincides with the WNW-ESE structural band comprising the Nogueras Zone (Figure 5b). The equivalent map along the N110 E direction magnifies the positive gravity anomaly 5 (Figure 5c).

5. Gravity Modeling

5.1. Density Properties

Table 1 shows the range and main statistics (arithmetic mean, standard deviation, and mode) of the measured density of representative rocks. They have been grouped into 13 rock units ranging between the Cambrian and the

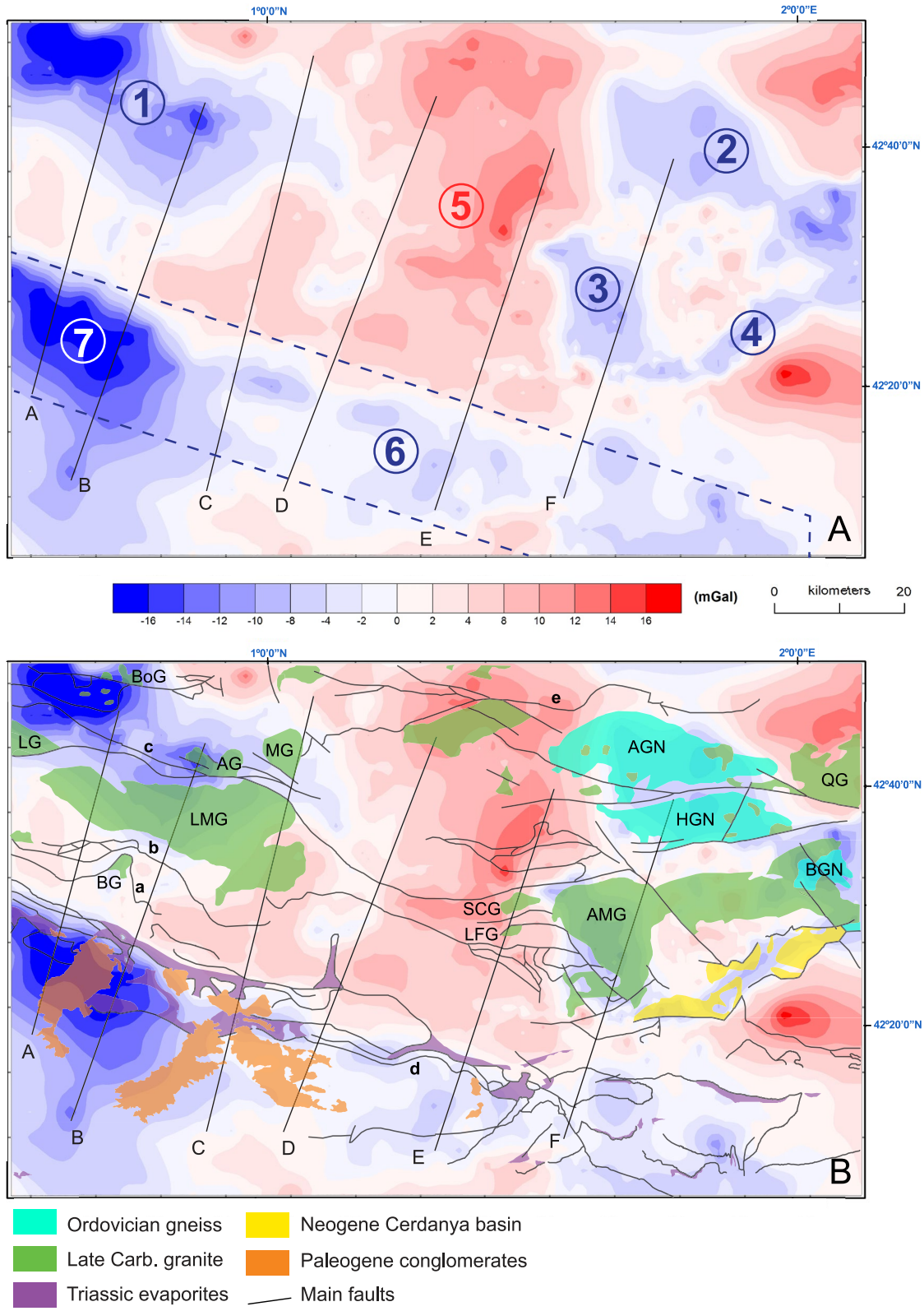

Figure 4. (a) Residual anomaly map of the study area. Main gravity minima and maximum are labeled to facilitate their description through the text. Contour interval is 2.0 mGal. (b) Residual anomaly map of the study area superposed with the main structures (labeled as in Figure 2B), main igneous bodies (labeled as in Figure 2B) and Triassic evaporitic outcrops of the study area. The location of the modeled sections A-A' to F-F' is shown.

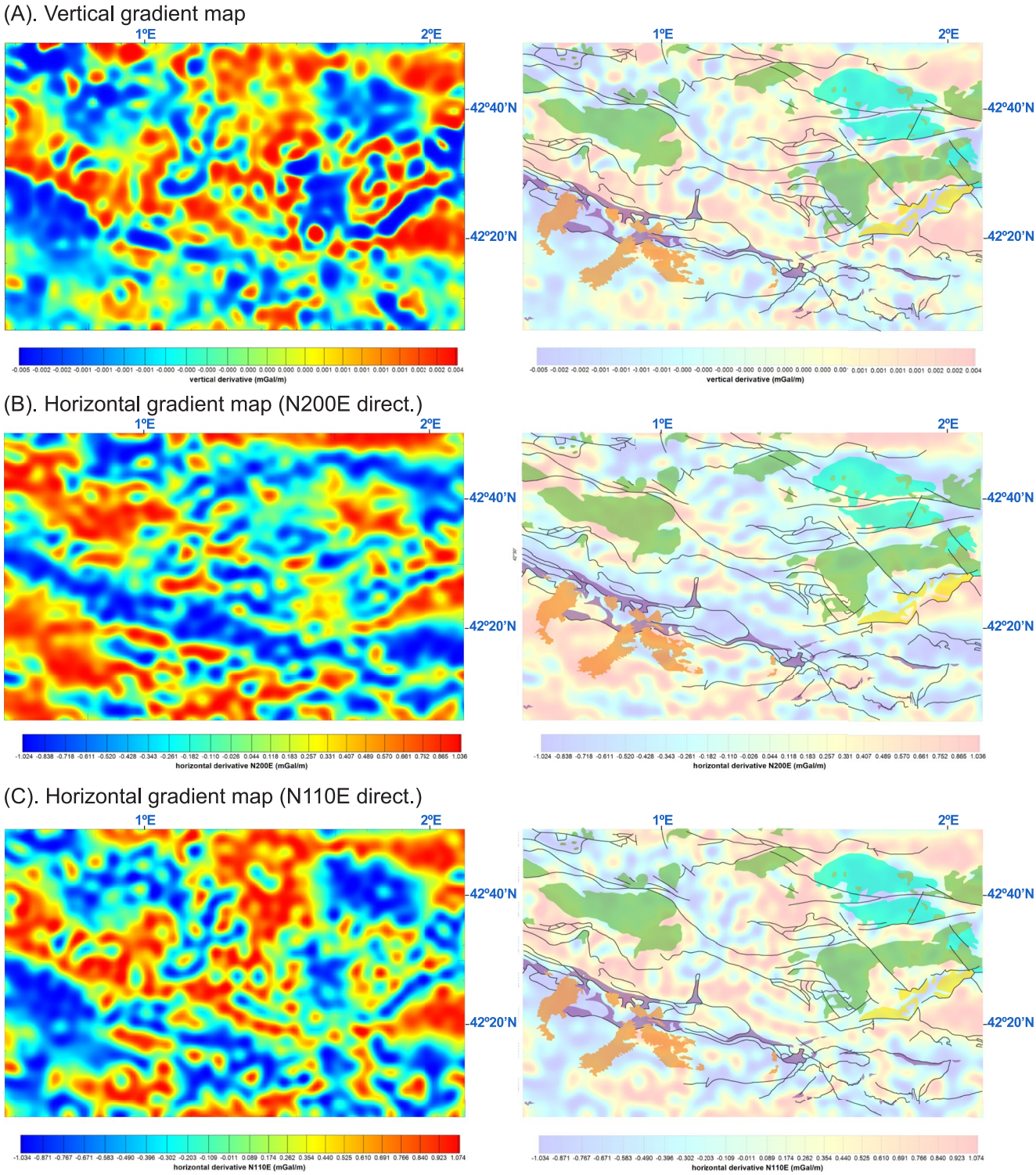

Figure 5. (a, b, c) Vertical, N200 E and N110 E horizontal gravity residual gradients. To the right, same maps superposed with the main structures (labeled as in Figure 2B), main igneous bodies (labeled as in Figure 2B) and Triassic evaporitic outcrops of the study area. Maps covering the same area as maps of Figures 3 and 4.

Oligocene-Neogene. Density was measured on 526 irregular non-weathered samples using the double weighting method (standard UNE-EN, 1936, p. 2007) obtaining the bulk density from each of them. All density values range between 1.85 and 3.03 g/cm^3. The highest density mean values of 2.69, 2.68 and 2.67 g/cm^3 correspond to the Devonian, pre-Stephanian Carboniferous, and Cambro-Ordovician rocks, respectively (Table 1). Upper Triassic

Table 1
Density Values (g/cm³) of Sampled Rocks and Statistics

Units	N	Mean (g/cm³)	Standard deviation (g/cm³)	Mode (g/cm³)	Range (g/cm³)
Cambro-Ordovician	75	2.67	0.08	2.68	2.35–2.81
Silurian	29	2.45	0.19	2.44	2.04–2.74
Devonian	86	2.69	0.102	2.69	2.41–3.03
Pre-Stephanian Carboniferous	5	2.68	0.013	2.70	2.67–2.7
Late Carboniferous-Permian	52	2.52	0.182	2.57	1.85–2.82
Early Triassic	24	2.58	0.110	2.69	2.31–2.69
Middle-Late Triassic	39	2.40	0.313	2.47	1.93–3.00
Jurassic-Late Cretaceous	17	2.66	0.059	2.65	2.51–2.78
Late Cretaceous	32	2.59	0.094	2.69	2.34–2.7
La Maladeta granite	48	2.65	0.093	2.64	2.29–2.89
Andorra-Mont Louis granite	58	2.63	0.051	-	2.50–2.74
Cenozoic	7	2.65	0.024	-	2.62–2.68
Ordovician gneiss	54	2.62	0.064	-	2.39–2.78

and Silurian rocks are the less dense ones, with mean density values of 2.40 and 2.45 g/cm^3. The ranges of each rock unit vary widely, being the Middle-Upper Triassic rocks the unit showing the largest range (i.e., between 1.93 and 3.00 g/cm^3). This wide range responds to the high variety of lithologies included in the Middle-Upper Triassic unit; evaporites, mudstones, lutites, limestones, dolostones, and dolerites. Pyrenean pre-Cambrian rocks crop out to the East of the study area (e.g., Padel et al., 2018), but no samples have been collected in this work. We interpret that they could be present at depth in the upper crust in our sections and have been assigned a density value of 2.70 g/cm^3. The density of collected samples indicates density mean values of 2.65 and 2.63 g/cm^3 for the La Maladeta and Andorra-Mont Louis granites, respectively, and 2.62 g/cm^3 for the Ordovician gneisses (Table 1).

5.2. Geological Cross Section Construction

Six almost parallel sections (A-A' to F-F') have been selected for modeling in order to cover the entire study area. Sections strike N010 E and N018 E, thus being perpendicular to most structures, are ~68–80 km long and keep a distance of ~20 km. Sections A and B were already created and modeled in a previous work (Clariana et al., 2021). The same geological units shown in the geological map of Figure 2 are considered in the cross sections.

Sections consist of composite geological cross sections constructed taking into account field data, surface geological data coming from geological maps (1:50.000 scale, MAGNA series, Instituto Geológico y Minero de España, and the geologic digital continuous map of Catalunya from Institut Cartogràfic i Geològic de Catalunya), well data (Tamurcia-1, Cajigar-1, Erinyà-1, San Corneli-1, Bóixols-1, Comiols-1, and Isona-1; Lanaja, 1987) (see well location in Figure 2) and previous interpreted cross sections from several authors (Table 2).

5.3. Processing and Interpretation of Modeled Sections

Forward gravity modeling was carried out using the GM-SYS module (implemented in the Oasis Montaj® software by Geosoft), which calculates the gravimetric response of given density models with an algorithm based on Talwani et al. (1959) and Won and Bevis (1987). The modeling has been carried out through a feedback process between geology and gravity that ended when the gravimetric response of each cross section (i.e., calculated gravity data) fitted the observations (i.e., observed gravity data). The different layers of each model were extended far enough at the end of the profiles to avoid edge effects. Since the density values are well constrained by laboratory measurements, in order to adjust the observed anomalies, we kept the mean densities fixed and modified

Table 2
Data Considered for the Construction of All Sections: Coordinates, Geological Maps, Wells and Previous Interpreted Cross Sections

Section	Coordinates ETRS89 H31	Geological maps	Well data	Previous cross-sections
Section A-A'	North X: 313,500,014 Y: 4,735,852,718 South X: 300,077,947 Y: 4685835,61	-García-Sansegundo et al. (2013)-MAGNA 118-bis148 -Ríos-Aragües et al. (2002)-MAGNA 180. -García-Senz and Ramirez-Merino (2009)-MAGNA 213. -López-Olmedo and Ardevol (2016)-MAGNA 251. -Alta Ribagorça-ICGC (2007).	-Tamurcia-1 (projection)	-García-Sansegundo (1992). -García-Senz (2002). -Teixell and Muñoz (2000). -Izquierdo-Llavall et al. (2013).
Section B-B'	North X: 326,764,021 Y: 4730763,27 South X: 306,125,282 Y:4,672,572,645	-Sanz-López and Palau (2013)-MAGNA 149. -Martín-Parra et al. (2016)-MAGNA 181. -Rosell (1994)-MAGNA 252. -Alta Ribagorça-ICGC (2007).	-Cajigar-1 (projection) -Tamurcia-1 (projection)	-Poblet (1991). -Soler et al. (1998). -Gil-Peña and Barnolas (2001). -García-Senz (2002). -Teixell and Muñoz (2000). -Saura et al. (2016).
Section C-C'	North X: 343,484,853 Y:4,737,960,244 South X: 327,022,759 Y:4,670,932,804	-Sanz-López and Palau (2013)-MAGNA 149. -Martín-Parra et al. (2016)-MAGNA 181. -Rosell (1994)-MAGNA 252. -Muñoz et al. (2009). -Muñoz et al. (2010). -Pallars-Sobirà-ICGC (2007). -Pallars-Jussà-ICGC (2007).	-Erinyà-1 -San Corneli-1 (projection)	-García-Senz (2002). -Mencos et al. (2015). -Muñoz et al. (2018). -Beamud et al. (2010). -Saura (2004).
Section D-D'	North X:362,146,385 Y: 4731097,02 South X: 338873,82 Y: 4,670,849,247	-Clariana (2015). -Muñoz et al. (2010). -Pallars-Sobirà-ICGC (2007). -Pallars-Jussà-ICGC (2007).	-Bóixols-1 (projection)	-Poblet (1991). -Muñoz (1992). -Mencos et al. (2015). -Gil-Peña and Barnolas (2004). -Saura (2004).
Section E-E'	North X: 380598,66; Y:4723660,49 South X:362674,16 Y: 4669353,45	-Clariana (2015). -Margalef (2015). -Alt-Urgell-ICGC (2007).		-Poblet (1991). -Vergés (1993). -García-Senz (2002). -Saura (2004). -Muñoz et al. (2018). -Clariana (2015). -Margalef (2015). -Casas et al. (2019).
Section F-F'	North X:399,003 Y:4,722,092 South X: 382,067 Y: 4,669,801	-Cirés et al. (1994). MAGNA 217. -Martínez et al. (2020). MAGNA 254. -Alt-Urgell-ICGC (2007).		-Cirés et al. (1990). -Soler (1990). -Poblet (1991). -Vergés (1993). -Margalef (2015).

the depth geometries in areas with scarce subsurface data. In some cases, when using the mean density was incompatible with a geological geometry, we modified the densities within the range of the petrophysical data (Table 1). The RMS fitting error (Root Mean Square of the difference between calculated and observed anomalies) in the six sections ranged between 0.55 and 1.3 mGal, less than 7% of the observed anomaly amplitudes. The most prominent misfits are small and correspond to the lack of a denser coverage of gravity stations in the Middle-Upper Triassic diapirs.

All sections, except the easternmost section F-F', cross the same structural units. From South to North these units are (Figure 6): the Montsec and Bóixols thrust sheets included in the South Pyrenean Zone and the Nogueras Zone and the Orri and Nogueras thrust sheets belonging to the Axial Zone. Section F-F' crosses from South to North, the Cadí, Pedraforca, and Bóixols thrust sheets in the South Pyrenean Zone and the Orri and Noguera's thrust sheets in the Axial Zone. All sections show at their southern sector an autochthonous succession of Paleogene sediments in continuation with the Ebro foreland basin underneath the basal Pyrenean southern thrust as

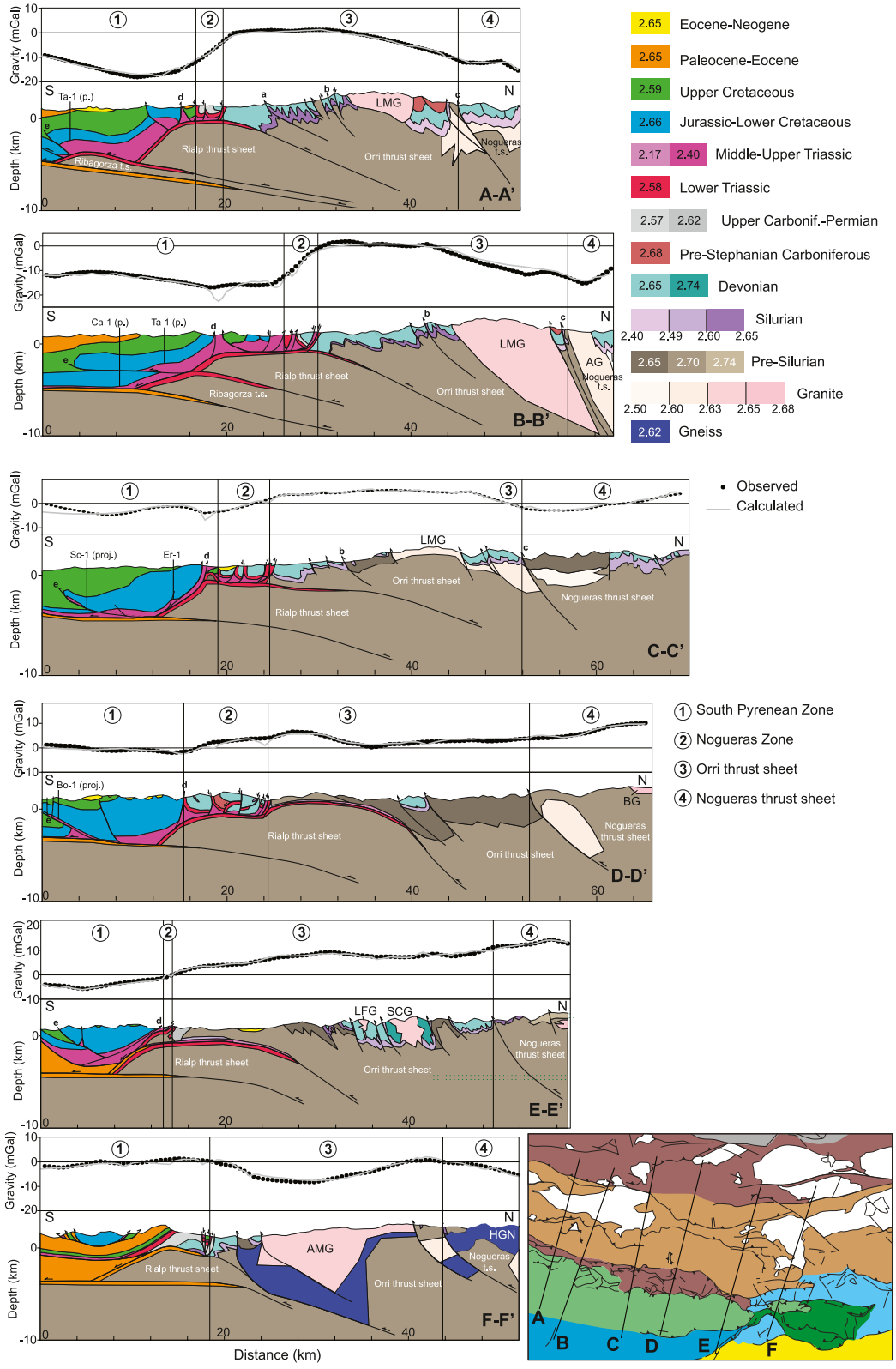

Figure 6. A-A' to F-F' modeled sections. Both the observed (points) and calculated (gray line) residual gravity anomalies are shown on top of each model section. See location of sections on Figure 2. Density values are in g/cm^3. When different density values are used in the same section, they are indicated on the caption. A schematic geologic map is also shown to help following results. Ourcropping granites are labeled according to Figure 2.

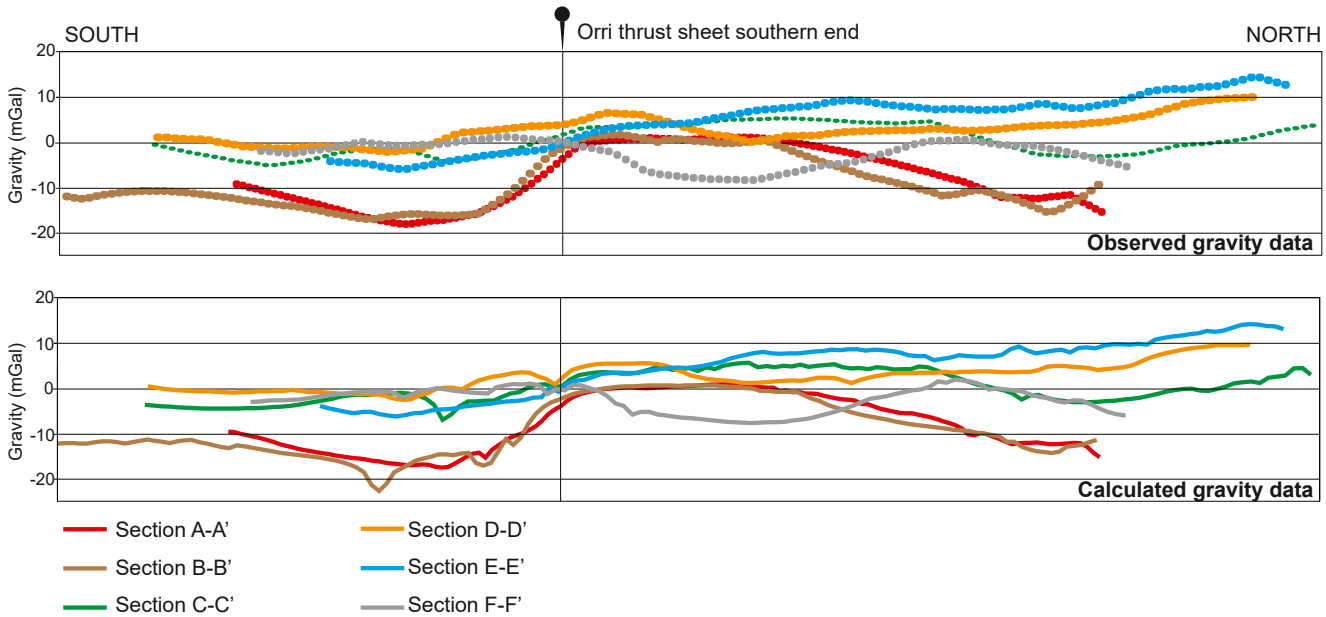

Figure 7. Calculated and observed gravity data of all sections together. All curves have been fixed in the southern end of the Orri thrust sheet.

evidenced by well (data projected from Comiols-1 and Isona-1 wells; see Figure 2 for location) and seismic data (e.g., Muñoz et al., 2018). The depth of this autochthonous succession ranges between 3,500 and 5,000 m showing a general slight westwards deepening following data and results obtained by Muñoz et al. (2018). The cut-off line between the Paleogene autochthonous succession and the south Pyrenean basal thrust cannot be delineated exactly from the available seismic data, but it can be mapped northwards of the branch line between the southernmost basement-involved thrust sheets and the south pyrenean basal thrust (see Muñoz et al., 2018).

In general, gravity data fit well with the proposed geometry interpreted by previous authors at the different parts of all composite sections. Most sectors showed the observed residual gravity data coinciding with the calculated one (Figure 6). The changes done in the sections to fit the calculated with the observed gravity data can be grouped into: (a) areal changes in the Middle-Upper Triassic evaporites at depth in the South Pyrenean Zone in areas without proximal well data, (b) subsurface areal changes in the outcropping granites and gneisses, (c) addition of buried granites in areas with surface evidences of their presence (e.g., northern sector of section A-A'), (d) addition of buried granites without surface evidences of their presence (e.g., northern sector of sections D-D' and F-F'), (e) presence of a thin layer of Middle-Upper Triassic evaporites at depth in the Orri thrust sheet in sections D-D' and E-E' inferred from the outcrops of Middle-Upper Triassic evaporites in the Rialp tectonic window (see Figure 2), (f) addition of a gneiss under the Andorra-Mont Louis granite (section F-F') already suggested by surface evidences (Denèle et al., 2014; Guitard et al., 1996), and (g) density value changes in the Middle-Upper Triassic (between 2.17 and 2.40 g/cm^3), Upper Carboniferous-Permian (between 2.57 and 2.62 g/cm^3), Silurian (between 2.40, 2.49, 2.60, and 2.65 g/cm^3), pre-Silurian (between 2.65, 2.70, and 2.74 g/cm^3) and granite (between 2.50, 2.60, 2.63, 2.65, and 2.68 g/cm^3) rocks considering the ranges obtained from collected samples (Table 1).

5.3.1. South Pyrenean Zone

The residual anomaly map shows a very strong along-strike variation of gravity residual values in the South Pyrenean Zone (Figure 4). The gravity low 1 shows a similarly observed gravity curve in sections A-A' and B-B' reaching values of −18 and −16 mGal, respectively. In section A-A', most of this gravity low does not correspond to Triassic evaporites at the surface, but its high amplitude suggests a large volume of this lithology at depth (Figure 6). The observed residual gravity curves of sections C-C', D-D' and F-F' show similar behavior, with data ranging around 0 mGal (Figure 7) which have been interpreted as linked to smaller volumes of Triassic evaporites at depth with respect to sections A-A' and B-B' (Figure 6). Section E-E', which shows lower gravity values ranging roughly between −5 and −2 mGal, has been modeled with an intermediate volume of Triassic

evaporites at depth (Figure 6). The modeled cross sections showing higher thicknesses of Triassic evaporites in the South Pyrenean Zone coincide with thinner Jurassic-Lower Cretaceous succession. The northern part in all curves, except that corresponding to section F-F', shows an upward trend toward higher gravity values. These upward trends match at depth with the southernmost leading edges of the youngest basement-involved thrust sheets; the Rialp and Ribagorza thrust sheets in sections A-A' and B-B' and the Rialp thrust sheet in sections C-C', D-D', and E-E' (Figure 6).

5.3.2. Nogueras Zone

Sections show a lateral variation on the geometry and width of the Nogueras Zone as previous authors have pointed out (Izquierdo-Llavall et al., 2018; Muñoz, 1992; Saura, 2004; Saura & Teixell, 2006; Seguret, 1972). Modeled sections also show that, in order to match the observed and calculated gravity data, an along-strike variation on the depth reached by the different thrust slices forming the Nogueras Zone is necessary. Sections C-C' and D-D' show a wider and deeper set of structures belonging to the Nogueras Zone with respect to sections A-A' and B-B'. Section E-E' only crosses the easternmost end of a small thrust slice of this unit (Figure 6). Modeled sections also show that the position of the Nogueras Zone must coincide, with a flat floor thrust (Figure 6). The depth to this flat of the floor thrust varies along-strike in parallel with the size of the thrust slices of the Nogueras Zone between 2,200 and 1,400 m-depth in sections D-D' and A-A', respectively.

The observed and calculated gravity curves of modeled sections crossing the Nogueras Zone show in all cases an increasing trend toward its limit with the Orri basement thrust sheet to the North. It is worth noting that the gravity minimum 7 (located in the South Pyrenean Zone) coincides with the western slices of the close Nogueras Zone that form a narrower band (sections A-A' and B-B'). Whereas the eastern half of the Nogueras Zone, outcropping as a much wider band, is not accompanied by such a gravity minimum (Figure 4).

5.3.3. Orri and Nogueras Thrust Sheet

Regarding the Orri unit, all sections, except F-F', coincide at their southern half with positive gravity residual values. These positive values show a discontinuous roughly Pyrenean WNW-ESE trend interrupted by several perpendicular minima of negative values (Figure 4). Sections A-A', B-B' and C-C' cross the gravity low 1 which coincides with the outcrops of the La Maladeta, Arties and Marimanha granites. The eastern end of the La Maladeta granite corresponds with a slight relative gravity high (section C-C'). In order to adjust the observed and calculated gravity curves a lower density value was chosen for the La Maladeta granite there. Section D-D' also shows a relative gravity minimum of positive values at the northern half of the Orri thrust sheet, whereas section E-E' displays higher positive values in equivalent positions (Figure 6). Section F-F' shows a different behavior; it traverses the gravity minimum 3 coinciding with the outcrop of the Andorra-Mont Louis granite and a gravity relative maximum between gravity lows 2 and 3 (Figure 6). In general, outcrops of Cambro-Ordovician rocks in the Orri thrust sheet are more abundant in the studied area toward the East, and the comparison of the observed and calculated gravity curves roughly highlights this tendency (i.e., higher gravity values toward the East) (Figure 7). In the Nogueras thrust sheet, the observed and calculated gravity curves of all sections also show the same tendency. Sections A-A' and B-B' display the lowest negative gravity values; in section B-B' they coincide with the outcrop of Arties granite and in section A-A' they have been interpreted to be linked to a buried granite at depth possibly related to the Bossost granite located to the north (Figure 6). Except for values of section F-F', sections C-C', D-D' and E-E' show a gradual increment of gravity values in the Nogueras thrust sheet (Figure 7).

6. Implications and Discussion

6.1. Along-Strike Gravity Differences in the Bóixols Thrust Sheet

One of the most remarkable features that can be observed in the residual anomaly map of the study area is the presence of the gravity low 7 located in the Bóixols thrust sheet (Figure 4). Toward the East, the Bóixols thrust sheet still coincides with gravity negative values, but much higher. According to the modeled cross sections, a gravity minimum 7 is interpreted as related to an important volume of Middle-Upper Triassic rocks at depth (Figure 6). Exploration wells located in that area (i.e., Tamurcia-1 and Cajigar-1; Lanaja, 1987) reached the Triassic evaporites but they did not cross the whole unit to infer its total thickness. It is worth noting that the modeled cross sections show an inverse proportion between the thickness of the Middle-Upper Triassic rocks and that of the Jurassic-Lower Cretaceous rocks. The westernmost sections (A-A' and B-B') show the

higher thickness of Middle-Upper Triassic rock and lower thickness of Jurassic-Lower Cretaceous rocks when compared with sections that traverse the eastern half of the Bóixols thrust sheet, which show the lower thickness of Middle-Upper Triassic rock and higher thickness of Jurassic-Lower Cretaceous rocks. This relationship could point to a lateral westward migration of the Triassic evaporites due to differential loading prior to the Cenozoic Alpine compression and probably to an increase in early diapirism to the West (e.g., Saura et al., 2016). Unraveling the pre-compressional thickness variations of the Triassic evaporites inside the Pyrenean range constitutes a difficult task due to the subsequent development of compressional structures and possible across- and/or along-strike evaporitic flows during its syn-rift, post-rift, and compressional stages (e.g., Burrel & Teixell, 2021; García-Senz, 2002; Santolaria et al., 2016; Storti et al., 2007). A visualization of the volumes of Triassic evaporites at depth based on gravity data could help to solve the pre-compression scenario.

At depth, this gravity low 7 also coincides with the presence of the Ribagorza basement thrust sheet in the modeled cross sections A-A' and B-B' (Figure 6). The Ribagorza basement thrust sheet constitutes the youngest basement thrust sheet in the footwall of the Rialp thrust sheet at this sector (e.g., Muñoz et al., 2018). Its formation could be favored by the presence of an important volume of Middle-Upper Triassic evaporites there, as the Bóixols and Montsec cover thrust sheets would have been already emplaced, and/or the occurrence of a thinnest Jurassic-Lower Cretaceous succession at this portion of the Bóixols thrust sheet. To the East, the thicker Jurassic-Lower Cretaceous deposits could prevent the southwards propagation of basement thrusts and the formation of the Ribagorza basement thrust sheet. The emplacement of the Bóixols and Montsec thrust sheets is dated from Late Santonian to Maastrichtian time and from Ilerdian to Cuisian time, respectively (Bond & McClay, 1995; Farrell et al., 1987; García-Senz, 2002; Garrido-Megías, 1973; Nijman & Nio, 1976; Simó, 1986; Teixell & Muñoz, 2000; Verges & Munoz, 1990), whereas the Rialp and Ribagorza basement thrust sheets have been interpreted to be emplaced after the Rupelian (Muñoz, 2002).

Another remarkable feature arises from the coincidence between the location of the northern boundary of the gravity minimum 7 with the sector of the Nogueras Zone where it is narrower and characterized by strongly stacked and rotated minor thrust units (Figure 4b). Toward the East, the Nogueras Zone is much wider and its thrust slices are larger and show lower dips. The emplacement of the Nogueras basement thrust sheet has been dated as Late Cretaceous to Middle Eocene (Muñoz, 1992), but the thrust slices belonging to the Nogueras Zone were emplaced and were tilted later, between the Late Eocene and Early Oligocene (Muñoz, 2002; Saura & Teixell, 2006). When the small units of the Nogueras Zone started to emplace at the Late Eocene, the Bóixols and Montsec thrust sheets were already emplaced and probably, the western half of the Bóixols thrust sheet already presented higher volumes of Triassic evaporites at depth due to evaporitic flow during the syn-rift, post-rift stage and compressional stage previous to the Late Eocene. The fact that the western half of the Bóixols thrust sheet coincides with higher volumes of Triassic evaporites at depth and the presence of steeper and narrower thrust slices in the Nogueras Zone suggests that the Triassic salt distribution could influence the formation and geometry of the Nogueras Zone structures. García-Senz and Muñoz (2019) already suggested the presence of Late Jurassic-Early Cretaceous evaporitic salt walls coinciding with the location of the Nogueras Zone. An along-strike variation on the geometry of these salt walls derived from variable volumes of Triassic evaporites prior to their emplacement could have controlled the geometry of the thrust slices of the Nogueras Zone.

Finally, another feature derived from the modeled sections is that thrust slices belonging to the Nogueras Zone arrange above a flat floor thrust in all modeled sections. This geometry is similar to the geometry interpreted along the Ribagorzana valley (to the West) by Muñoz et al. (2018) and contrasts with that interpreted along the Pallaresa valley (to the East) located these units on a ramp of the floor thrust (Muñoz et al., 2018).

6.2. Variability of Gravity Values in the Orri and Nogueras Thrust Sheets

The residual anomaly map of the Orri and Nogueras thrust sheets of the study area reflects two different patterns. (a) Pyrenean WNW-ESE elongated gravity lows and highs more evident at the western half and easternmost sector of the study area (gravity lows 1 and 2) and (b) a complex pattern defined by WNW-ESE and NNE-SSW to N-S oriented gravity maxima and minima (gravity lows 3 and 4 and gravity high 5) in the central sector of the study area (Figure 4). The gravity minima 1, 2, and 3 coincide at the surface with outcrops of plutonic rocks (Figure 4). All these plutonic bodies with exception of Andorra-Mont Louis granite give a gravity response coinciding with WNW-ESE elongated negative anomalies, parallel to the main Pyrenean trend. It is worth noting that the La Maladeta and Andorra-Mont Louis granites point to a different gravity response probably reflecting differences

in their density values (see Table 1) and geometry at depth. The results obtained from gravity modeling show that the La Maladeta granite displays a laccolithic shape at its ends (sections A-A' and C-C') with its basal contact deepening to the North (Figure 6) and the Andorra Mont-Louis granite has a more batholitic shape (section F-F'; Figure 6). Section B-B' shows an elongated vertical shape for the Arties granite to fit the observed and calculated gravity curves. Below the Andorra Mont-Louis granite, the presence of a gneiss dome of lower density has been interpreted to match both gravity curves (see section F-F'; Figure 6). This feature has already been suggested by previous authors (Debon et al., 1996; Denèle et al., 2014) based on geological evidence. Ortogneisses as those surrounding the Andorra Mont-Louis granite display slightly lower densities than the density mean value obtained for this granite (see Table 1). The presence of granitic bodies both coinciding with surface outcrops (i.e., Marimanha, Bassiès, La Fontaneda, and Santa Coloma granites; Figures 2 and 6) and with buried granites of lesser volume compared to the modeled volume of La Maladeta and Andorra Mont-Louis granites, has been interpreted for sections C-C', D-D' and E-E' (Figure 6). Also the Bono granite (Figure 2) coincides with part of a small N-S gravity low suggesting its higher volume at depth (Figure 4). The gravity high 5 does not coincide with any structural trend at surface and could reflect inherited Variscan or pre-Variscan compositional crustal variations following this trend. Previous authors have suggested the important role played by lateral variations of the rheological inheritance and/or inherited faults on the structural architecture of the Pyrenees (e.g., Chevrot et al., 2014; Chevrot et al., 2018; Jammes et al., 2014). To the South of the Orri thrust sheet, Triassic evaporites crop out in the Rialp window (e.g., Muñoz, 1992). A gravity low showing an NNE-SSW orientation appears to the North of the Rialp window (Figures 2 and 4) pointing out a possible relationship.

Figure 7 shows all observed and calculated gravity data along the modeled sections together to facilitate their comparison. In the southern half of the Orri thrust sheet, all curves with exception of section F-F' show gravity values ranging between 0 and 6 mGal, a relatively narrow range. This range grows toward the North (i.e., between −13 and 14 mGal; Figure 7). The highest gravity values are shown in the northernmost part of section E-E'. This area coincides with outcrops of high-grade metamorphic rocks; biotite zone, garnet zone, andalusite-staurolite-cordierite zone, staurolite out zone, and sillimanite zone (Alías, 1995; Clariana, 2015; Guitard et al., 1996). Cambro-Ordovician samples of this area show density values ranging between 2,610 and 2,744 kg/m^3, similar to the mean density value obtained for these rocks in the whole study area (Table 1). The density of metamorphic rocks does not always show high values because they strongly depend on the composition, density of the protolith, the degree of metamorphism, and thermodynamic conditions and processes (Schön, 2011). The residual gravity maximum 5 (Figure 4b) might be linked to higher density rocks located at depth.

7. Conclusions

In this work we use gravity, petrophysical and geological data to constrain the geometry of the upper crust of the Central Pyrenees. The study area lies on a long-wavelength negative Bouguer anomaly ranging between −120 and −67.5 mGal together with several relative gravity maxima and minima following a complex pattern. The residual anomaly map shows values ranging between −18 and 18 mGal and highlights two areas separated by a Pyrenean-oriented limit coinciding with the Axial Zone southern termination.

In general, gravity data fit well with the geometry proposed by previous authors at the different parts of the six composite sections done for this work, except for; (a) different thicknesses and/or presence of Triassic evaporites at depth in the South Pyrenean Zone and Axial Zone, (b) different geometry at depth of the Late Variscan granites and Ordovician gneisses, (c) buried Late Variscan granites, with or without evidence of their presence, at the surface, and (d) the existence of a gneiss under the Andorra-Mont Louis granite. Our results highlight strong along-strike variations both (a) in the South Pyrenean Zone mainly due to different along-strike variations in the thicknesses of the Triassic evaporites and Mesozoic rocks and (b) in the Axial Zone linked to lithological and rheological variations in the Paleozoic rock and presence of igneous bodies. The across- and along-strike differences in the superficial and subsurface occurrence of Triassic evaporites have important implications for controlling the structural style in the Pyrenees and in the Axial Zone, the distribution of basement thrust sheets and igneous bodies are relevant to improving the understanding of the orogenic building process.

Data Availability Statement

Data supporting the conclusions can be obtained from the Digital.CSIC repository (http://hdl.handle.net/10261/254934 or https://doi.org/10.20350/digitalCSIC/14026) and in the Application SIGEOF (https://info.igme.es/SIGEOF/).

Acknowledgments
This work was funded by projects CGL2017-84901-C2-2-P funded by MCIN/AEI/10.13039/501100011033 and "ERDF A way of making Europe", PID2020-114273GB-C22 funded by MCIN/AEI/10.13039/501100011033 from the Spanish Ministry of Science and Innovation, and "Severo Ochoa" extraordinary grants for excellence IGME-CSIC (AECEX2021). The authors acknowledge the contribution of José María Llorente and Agustín González for the acquisition of the gravity data. This study represents a contribution to GeoAp Research Group (E01-20R) (Aragón Government). We thank the Editor Laurent Jolivet, and Esther Izquierdo-Llavall and one anonymous reviewer for suggestions and comments that helped to improve the paper.

References

Ali, M. Y., Watts, A. B., & Farid, A. (2014). Gravity anomalies of the United Arab Emirates: Implications for basement structures and infra-Cambrian salt distribution. *GeoArabia*, *19*(1), 143–158. https://doi.org/10.2113/geoarabia1901143

Alías, G. (1995). *El metamorfisme regional herciniá de les metapelites del sector Occidental dels macizos de l'Aston y de l'Hospitalet (Pirineu Central)*. PhD Thesis (p. 214). Universidad de Barcelona.

Alt, U. (2007). *Mapa geològic comarcal de Catalunya 1:50000*. Institut Cartogràfic i Geològic de Catalunya. (ICGC), used under the license CC BY 4.0".

Aranguren, A., Cuevas, J., Tubia, J. M., Román-Berdiel, T., Casas-Sainz, A., & Casas-Ponsati, A. (2003). Granite laccolith emplacement in the Iberian arc: AMS and gravity study of the La Tojiza pluton (NW Spain). *Journal of the Geological Society*, *160*(3), 435–445. https://doi.org/10.1144/0016-764902-079

Autran, A., Fonteilles, M., & Guitard, G. (1970). Relations entre les intrusions de granitoides, l'anatexie et le metamorphisme regional considerees principalement du point de vue du role de l'eau; cas de la chaine hercynienne des Pyrenees orientales. *Bulletin de la Societe Geologique de France*, *7*(4), 673–731. https://doi.org/10.2113/gssgfbull.s7-xii.4.673

Ayala, C., Bohoyo, F., Maestro, A., Reguera, M. I., Torné, M., Rubio, F., et al. (2016). Updated Bouguer anomalies of the Iberian Peninsula: A new perspective to interpret the regional geology. *Journal of Maps*, *12*, 1089–1092. https://doi.org/10.1080/17445647.2015.1126538

Ayala, C., Rey-Moral, C., Rubio, F. M., Pueyo, E. L., Casas, A. M., Clariana, P., et al. (2020). Nuevos datos gravimétricos en los Pirineos Centrales (NE de España). *Geogaceta*, *67*, 103–106.

Ayala, C., Rubio, F. M., Rey-Moral, C., Reguera, M. I., & Biete, C. (2019). Three-dimensional geophysical characterization of the La Rambla and Zafra de Záncara anticlines (Loranca basin, Central Spain). *Geophysical Prospecting*, *67*(3), 580–594. https://doi.org/10.1111/1365-2478.12745

Barnolas, A., & Gil-Peña, I. (2001). Ejemplos de relleno sedimentario multiepisódico en una cuenca de antepaís fragmentada: La Cuenca Surpirenaica. *Boletin Geologico y Minero*, *112*, 17–38.

Beaumont, C., Muñoz, J. A., Hamilton, J., & Fullsack, P. (2000). Factors controlling the Alpine evolution of the central Pyrenees inferred from a comparison of observations and geodynamical models. *Journal of Geophysical Research*, *105*, 8121–8145. https://doi.org/10.1029/1999JB900390

Blakely, R. J. (1996). *Potential theory in gravity and magnetic applications*. Cambridge university press.

Bond, R. M. G., & McClay, K. R. (1995). Inversion of a Lower Cretaceous extensional basin, south central Pyrenees, Spain. In J. G. Buchanan, & P. G. Buchanan (Eds.), *Basin Inversion* (Vol. 88, pp. 415–431). Geological Society, London, Special Publications. https://doi.org/10.1144/GSL.SP.1995.088.01.22

BRGM. (2009). *Bureau de Recherches Géologiques et Minières)*. Banque Gravimétrique de la France.

Burrel, L., & Teixell, A. (2021). Contractional salt tectonics and role of pre-existing diapiric structures in the Southern Pyrenean foreland fold–thrust belt (Montsec and Serres Marginals). *Journal of the Geological Society*, *178*(4). https://doi.org/10.1144/jgs2020-085

Cabrera, L., Roca, E., & Santanach, P. (1988). Basin formation at the end of a strike-slip fault: The Cerdanya basin (eastern Pyrenees). *Journal of the Geological Society*, *145*(2), 261–268. https://doi.org/10.1144/gsjgs.145.2.0261

Calcagno, P., Chilès, J. P., Courrioux, G., & Guillen, A. (2008). Geological modelling from field data and geological knowledge: Part I. Modelling method coupling 3D potential-field interpolation and geological rules. *Physics of the Earth and Planetary Interiors*, *171*(1–4), 147–157. https://doi.org/10.1016/j.pepi.2008.06.013

Calvet, F., Anglada, E., & Salvany, J. M. (2004). El Triásico de los Pirineos. In J. A. Vera (Ed.), *Geología de España* (pp. 272–274). SGE-IGME.

Calvín, P., Santolaria, P., Casas, A. M., & Pueyo, E. L. (2018). Detachment fold vs. ramp anticline: A gravity survey in the southern pyrenean front (External Sierras). *Geological Journal*, *53*(1), 178–190. https://doi.org/10.1002/gj.2884

Campanyà, J., Ledo, J., Queralt, P., Marcuello, A., Liesa, M., & Muñoz, J. A. (2011). Lithospheric characterization of the Central Pyrenees based on new magnetotelluric data. *Terra Nova*, *23*(3), 213–219.

Campanyà, J., Ledo, J., Queralt, P., Marcuello, A., Liesa, M., & Muñoz, J. A. (2012). New geoelectrical characterisation of a continental collision zone in the West-Central Pyrenees: Constraints from long period and broadband magnetotellurics. *Earth and Planetary Science Letters*, *333*, 112–121.

Canva, A., Thinon, I., Peyrefitte, A., Couëffé, R., Maillard, A., Jolivet, L., et al. (2020). The Catalan magnetic anomaly: Its significance for the crustal structure of the Gulf of Lion passive margin and relationship to the Catalan transfer zone. *Marine and Petroleum Geology*, *113*, 104174. https://doi.org/10.1016/j.marpetgeo.2019.104174

Capellà, I. (1991). *Variació de l'estil estructural a l'Hercinià del Pirineu. Infrastructura – zona de Transició – Suprastructura*. PhD Thesis (p. 279). Univ. Autónoma de Barcelona.

Casas, A., Kearey, P., Rivero, L., & Adams, C. R. (1997). Gravity anomaly map of the Pyrenees region and comparison of the deep geological structure of the western and east Pyrenees. *Earth and Planetary Science Letters*, *150*, 65–78. https://doi.org/10.1016/s0012-821x(97)00087-3

Casas, A., Torné, M., & Banda, E. (1987). *Mapa gravimètric de Catalunya, scale 1: 500000* (p. 135). Servei Geològic de Catalunya (DPT i OP), ICC.

Casas, J. M., Clariana, P., García-Sansegundo, J., Margalef, A., Puddu, C., Sanz-López, J., et al. (2019). The Pyrenees. In C. Quesada, & J. Oliveira (Eds.), *The geology of Iberia: A Geodynamic approach. Regional geology Reviews* (pp. 335–259). Springer. https://doi.org/10.1007/978-3-030-10519-8_8

Casas-Sainz, A., & Faccenna, C. (2001). Tertiary compressional deformation of the Iberian plate. *Terra Nova*, *13*(4), 281–288. https://doi.org/10.1046/j.1365-3121.2001.00355.x

Chevrot, S., Sylvander, M., Diaz, J., Martin, R., Mouthereau, F., Manatschal, G., & Ruiz, M. (2018). The non-cylindrical crustal architecture of the Pyrenees. *Scientific Reports*, *8*(1), 1–8. https://doi.org/10.1038/s41598-018-27889-x

Chevrot, S., Sylvander, M., Diaz, J., Ruiz, M., & Paul, A., & PYROPE Working Group (2015). The Pyrenean architecture as revealed by teleseismic P-to-S converted waves recorded along two dense transects. *Geophysical Journal International*, *200*(2), 1096–1107. https://doi.org/10.1093/gji/ggu400

Chevrot, S., Villaseñor, A., Sylvander, M., Benahmed, S., Beucler, E., Cougoulat, G., et al. (2014). High-resolution imaging of the Pyrenees and Massif Central from the data of the PYROPE and IBERARRAY portable array deployments. *Journal of Geophysical Research: Solid Earth*, *119*(8), 6399–6420. https://doi.org/10.1002/2014jb010953

Choukroune, P., & ECORS team. (1989). The ECORS Pyrenean deep seismic profile reflection data and the overall structure of an orogenic belt. *Tectonics*, *8*, 23–39. https://doi.org/10.1029/tc008i001p00023

Cirés, J., Alías, G., Poblet, J. & Casas, J. M. (1990). La estructura del anticlinal de La Massana (Hercínico del Pirineo central). *Geogaceta*, *8*, 42–44.

Cirés, J., Roca, E., Domingo, F., Escuer-Sole, J., Sirvent-Artiaga, J. C., & Santanach, P. (1994). Mapa geológico Hoja nº 217 (Puigcerdà). In *Mapa Geológico de España E. 1: 50.000 (MAGNA)*. IGME.

Clariana, P. (2015). *Estratigrafía, estructura y su relación con el metamorfismo de la Zona Axial pirenaica en la transversal del noroeste de Andorra y comarcas del Pallars Sobirá y el Alt Urgell (Lleida)*. PhD Thesis (p. 195). Universidad de Oviedo.

Clariana, P., Soto, R., Ayala, C., Casas-Sainz, A. M., Román-Berdiel, T., Oliva-Urcia, B., et al. (2021). Basement and cover architecture in the Central Pyrenees constrained by gravimetric data. *International Journal of Earth Sciences*, 1–18.

Clerc, C., & Lagabrielle, Y. (2014). Thermal control on the modes of crustal thinning leading to mantle exhumation: Insights from the Cretaceous Pyrenean hot paleomargins. *Tectonics*, *33*(7), 1340–1359. https://doi.org/10.1002/2013tc003471

Cochelin, B., Chardon, D., Denèle, Y., Gumiaux, C., & Le Bayon, B. (2017). Vertical strain partitioning in hot Variscan crust: Syn-convergence escape of the Pyrenees in the Iberian-Armorican syntax. *Bulletin de la Societe Geologique de France*, *188*(6), 39. https://doi.org/10.1051/bsgf/2017206

Crombez, V., Hauser, J., Peeters, L., & Chopping, R. (2020). Understanding the gravity response variability of sedimentary basins using forward stratigraphic modelling. *Marine and Petroleum Geology*, *122*, 104698. https://doi.org/10.1016/j.marpetgeo.2020.104698

Daignières, M., Gallart, J., & Banda, E. (1981). Lateral variation of the crust in the north pyrenean zone. *Annals of Géophysics*, *37*(3), 453–456.

Debon, F., Enrique, P., & Autran, A. (1996). Magmatisme hercyniene In A. Barnolas& J. C.Chiron(Eds.), *Synthèse géologique at géophysique des Pyrénées* (Vol. 1, pp. 361–500). BRGM – ITGE.

Denèle, Y. (2007). Formation des dômes gneissiques hercyniens dans les Pyrénées: Exemple du massif de l'Aston-Hospitalet (Vol. *3*). Doctoral dissertation.

Denèle, Y., Laumonier, B., Paquette, J. L., Olivier, P., Gleizes, G., & Barbey, P. (2014). Timing of granite emplacement, crustal flow and gneiss dome formation in the Variscan segment of the Pyrenees. In K. Schulmann, J. R. Martínez-Catalán, J. M. Lardeaux, V. Janousêk, & G. Oggiano (Eds.), *The Variscan orogeny: Extent, Timescale and the Formation of the European Crust*. (Vol. 405, pp. 265–287). Geol. Soc. London Spec. Pub.

Devolvé, J. J. (1987). *Un bassin synorogénique varisque. Le Culm des Pyrénées centro-occidentales*. PhD Thesis. University of Toulouse.

Díaz, J., Pedreira, D., Ruiz, M., Pulgar, J. A., & Gallart, J. (2012). Mapping the indentation between the Iberian and Eurasian plates beneath the western Pyrenees/eastern Cantabrian mountains from receiver function analysis. *Tectonophysics*, *570*, 114–122.

ECORS-Pyrenees Team. (1988). Deep reflection seismic survey across an entire orogenic belt, the ECORS Pyrenees profile. *Nature*, *331*, 508–511.

Espurt, N., Angrand, P., Teixell, A., Labaume, P., Ford, M., de Saint Blanquat, M., & Chevrot, S. (2019). Crustal-scale balanced cross-section and restorations of the Central Pyrenean belt (Nestes-Cinca transect): Highlighting the structural control of Variscan belt and Permian-Mesozoic rift systems on mountain building. *Tectonophysics*, *764*, 25–45. https://doi.org/10.1016/j.tecto.2019.04.026

Evans, N. G. (1993). *Deformation during the emplacement of the Maladeta granodiorite Spanish Pyrenees*, PhD thesis. University of Leeds.

Farr, T. G., Rosen, P. A., Caro, E., Crippen, R., Duren, R., Hensley, S., & Alsdorf, D. (2007). The shuttle radar topography mission. *Reviews of Geophysics*, *45*(2). https://doi.org/10.1029/2005rg000183

Farrell, S. G., Williams, G. D., & Atkinson, C. D. (1987). Constraints on the age of movement of the Montsech and Cotiella thrusts, south central Pyrenees, Spain. *Journal of the Geological Society*, *144*(6), 907–914. https://doi.org/10.1144/gsjgs.144.6.0907

Fernández, M., Torné, M., & Zeyen, H. (1990). Modelling of thermal anomalies in the NW border of the Valencia Trough by groundwater convection. *Geophysical Research Letters*, *17*(1), 105–108.

Ford, M., & Vergés, J. (2021). Evolution of a salt-rich transtensional rifted margin, eastern North Pyrenees, France. *Journal of the Geological Society*, *178*(1). https://doi.org/10.1144/jgs2019-157

Forster, C., & Smith, L. (1989). The influence of groundwater flow on thermal regimes in mountainous terrain: A model study. *Journal of Geophysical Research*, *94*(B7), 9439–9451. https://doi.org/10.1029/jb094ib07p09439

Gallart, J., Banda, E., & Daignières, M. (1981). Crustal structure of the Paleozoic axial zone of the Pyrenees and transition to the north pyrenean zone. *Annals of Geophysics*, *37*(3), 457–480.

García-Sansegundo, J. (1990). Structure of the Paleozoic in the aran valley, axial zone, central Pyrenees. *Bulletin de la Societe Géologique de France*, *2*, 229–239.

García-Sansegundo, J. (1992). *Estratigrafía y estructura de la Zona Axial pirenaica en la transversal del Valle de Aran y de la Alta Ribagorça* (p. 167). Publicaciones especiales del Boletín Geológico y Minero.

García-Sansegundo, J., Poblet, J., Alonso, J. L., & Clariana, P. (2011). Hinterland – foreland zonation of the Variscan orogen in the central Pyrenees: Comparison with the northern part of the Iberian Variscan Massif. In J. Poblet, & R. J. Lisle (Eds.), *From Kinematic evolution and structural styles of Fold-and-thrust belts* (Vol. 349, pp. 169–184). Geological Society, London, Special Publications.

García-Sansegundo, J., & Ramírez Merino, J. I. (2013). *Mapa geológico de España E. 1:50.000, Hoja n° 118bis- 148 (Caneján- Viella), 2ª serie MAGNA*. Instituto Geológico y Minero de España.

García-Senz, J. (2002). *Cuencas extensivas del cretácico inferior en los Pirineos centrales, formación y subsecuente inversión*. PhD Thesis (p. 310). Universitat de Barcelona.

García-Senz, J., & Muñoz, J. A. (2019). South central Pyrenees: The Organyà rift basin. In C. Quesada, & J. Oliveira (Eds.), *The geology of Iberia: A Geodynamic approach. Regional geology Reviews* (pp. 182–190). Springer.

García-Senz, J., Pedrera, A., Ayala, C., Ruiz-Constán, A., Robador, A., & Rodríguez-Fernández, L. R. (2020). Inversion of the North Iberian hyperextended margin: The role of exhumed mantle indentation during continental collision. *Geological Society, London, Special Publications*, *490*(1), 177–198.

García-Senz, J., & Ramirez-Merino, J. I. (2009). *Mapa geológico de España E. 1:50.000, Hoja n° 213 (el Pont de Suert), 2ª serie MAGNA*. Instituto Geológico y Minero de España.

Garrido-Megías, A. (1973). *Estudio geológico y relación entre tectónica y sedimentación del Secundario y Terciario de la vertiente meridional pirenaica en su zona central (provincias de Huesca y Lerida)* (pp. 1–395). Ph.D. thesis. University of Granada.

Gil-Peña, I., & Barnolas, A. (2001). Superposición estructural hercínica y alpina en el borde occidental del domo de Pallassos (Noguera de Tor, Pirineo central). *Boletín Geológico y Minero de España*, *112*(3), 5–16.

Gil-Peña, I., & Barnolas, A. (2004). El domo del Orri (Pirineo Central): un pliegue – manto reactivado por la tectónica alpina. *Geotemas*, *6*(3), 267–270.
Gisbert, J. (1983). El Pérmico de los Pirineos españoles. In C. Martínez Díaz (Ed.), *Carbonífero y Pérmico de España*. X Congreso Internacional de Estratigrafía y Geología del Carbonífero (pp. 405–420).
Godin, L., & Harris, L. B. (2014). Tracking basement cross-strike discontinuities in the Indian crust beneath the Himalayan orogen using gravity data–relationship to upper crustal faults. *Geophysical Journal International*, *198*(1), 198–215. https://doi.org/10.1093/gji/ggu131
Goleby, B. R., Shaw, R. D., Wright, C., Kennett, B. L., & Lambeck, K. (1989). Geophysical evidence for'thick-skinned'crustal deformation in central Australia. *Nature*, *337*(6205), 325–330. https://doi.org/10.1038/337325a0
Guitard, G., Vielzeuf, D., & Martinez, F. (1996). Métamorphisme Hercynien. In A. Barnolas, & J. C. Chiron (Eds.), *Synthèse géologique at géophysique des Pyrénées* (Vol. 1, pp. 501–584). BRGM – ITGE.
ICC. (1987). *Mapa gravimètric de Catalunya 1:500.000 I* (Casas, A., Torné, M., & Banda, E., Servei Geològic de Catalunya). Institut Cartogràfic de Catalunya.
IGC-ICC-ICTJA-CSIC. (2012). *Mapa gravimètric de Catalunya 1:250.000*. Institut Geològic de Catalunya (IGC), Institut Cartogràfic de Catalunya. (ICC) i Institut de Ciències de la Terra Jaume Almera del Consell Superior d'Investigacions Científiques (ICTJA-CSIC).
Izquierdo-Llavall, E., Ayala, C., Pueyo, E. L., Casas, A. M., Oliva-Urcia, B., Rubio, F., et al. (2019). Basement-cover relationships and their along-strike changes in the linking zone (Iberian range, Spain): A combined structural and gravimetric study. *Tectonics*, *38*, 2934–2960. https://doi.org/10.1029/2018TC005422
Izquierdo-Llaval, E., Casas-Sainz, A. M., Oliva-Urcia, B. (2013). Heterogeneous deformation recorded by magnetic fabrics in the Pyrenean Axial Zone. *Journal of Structural Geology*, *57*, 97–113. http://dx.doi.org/10.1016/j.jsg.2013.10.005
Izquierdo-Llavall, E., Casas-Sainz, A. M., Oliva-Urcia, B., Villalaín, J. J., Pueyo, E., & Scholger, R. (2018). Rotational kinematics of basement antiformal stacks: Paleomagnetic study of the western Nogueras zone (central Pyrenees). *Tectonics*, *37*(10), 3456–3478.
Jammes, S., & Huismans, R. S. (2012). Structural styles of mountain building: Controls of lithospheric rheologic stratification and extensional inheritance. *Journal of Geophysical Research*, *117*(B10). https://doi.org/10.1029/2012jb009376
Jammes, S., Huismans, R. S., & Muñoz, J. A. (2014). Lateral variation in structural style of mountain building: Controls of rheological and rift inheritance. *Terra Nova*, *26*(3), 201–207. https://doi.org/10.1111/ter.12087
Jammes, S., Manatschal, G., Lavier, L., & Masini, E. (2009). Tectonosedimentary evolution related to extreme crustal thinning ahead of a propagating ocean: Example of the western Pyrenees. *Tectonics*, *28*(4). https://doi.org/10.1029/2008tc002406
Jessell, M. (2001). Three-dimensional geological modelling of potential-field data. *Computers & Geosciences*, *27*(4), 455–465. https://doi.org/10.1016/s0098-3004(00)00142-4
Kane, M. F. (1962). A comprehensive system of terrain corrections using a digital computer. *Geophysics*, *27*(4), 455–462. https://doi.org/10.1190/1.1439044
Labaume, P., Meresse, F., Jolivet, M., Teixell, A., & Lahfid, A. (2016). Tectonothermal history of an exhumed thrust- sheet- top basin: An example from the south Pyrenean thrust belt. *Tectonics*, *35*(5), 1280–1313. https://doi.org/10.1002/2016tc004192
LaFehr, T. R., & Nabighian, M. N. (2013). Fundamentals of gravity Exploration. https://doi.org/10.1190/1.9781560803058
Lago, M., Galé, C., Arranz, E., Vaquer, R., Gil, A., & Pocoví, A. (2000). Triassic tholeiitic dolerites ("ophites") of the el Grado diapir (Pyrenees, Huesca, Spain): Emplacement and composition. *Estudios Geológicos*, *56*, 3–18.
Lanaja, J. M. (1987). Contribución de la exploración petrolífera al conocimiento de la Geología de España (p. 465). IGME 17 maps.
Ledo, J., Ayala, C., Pous, J., Queralt, P., Marcuello, A., & Muñoz, J. A. (2000). New geophysical constraints on the deep structure of the Pyrenees. *Geophysical Research Letters*, *27*(7), 1037–1040. https://doi.org/10.1029/1999gl011005
López-Olmedo, F., & Ardevol, L. (2016). *Mapa geológico de España E. 1:50.000, Hoja n° 251 (Arén), 2ª serie MAGNA*. Instituto Geológico y Minero de España.
López-Sánchez, M., García-Sansegundo, J., & Martínez, F. (2019). The significance of early Permian and early Carboniferous U– Pb zircon ages in the Bossòst and Lys-Caillaouas granitoids (pyrenean axial zone). *Geological Journal*, *54*(4), 2048–2063. https://doi.org/10.1002/gj.3283
Marcén, M., Casas-Sainz, A. M., Román-Berdiel, T., Oliva-Urcia, B., Soto, R., & Aldega, L. (2018). Kinematics and strain distribution in an orogen-scale shear zone: Insights from structural analyses and magnetic fabrics in the Gavarnie thrust, Pyrenees. *Journal of Structural Geology*, *117*, 105–123.
Margalef, A. (2015). *Estudi estructural i estratigràfic del sud d'Andorra*. PhD Thesis (p. 172). Universitat de Barcelona.
Martínez, A., Losantos, M., Domingo, F., Samsó, J. M. A., Saula, E., Soriano, C., et al. (2020). *Mapa geológico de la Hoja nº 254 (Gósol). Mapa geológico de España E. 1: 50.000*. IGME. Segunda Serie (MAGNA).
Martínez, A., Vergés, J., & Muñoz, J. A. (1988). Secuencias de propagación del sistema de cabalgamientos de la terminación oriental del manto del Pedraforca y relación con los conglomerados sinorogénicos. *Acta Geológica Hispánica*, *23*(2), 119–127.
Martínez Catalán, J. R., Álvarez Lobato, F., Pinto, V., Gómez Barreiro, J., Ayarza, P., Villalaín, J. J., & Casas, A. (2012). Gravity and magnetic anomalies in the allochthonous Órdenes Complex (Variscan belt, northwest Spain): Assessing its internal structure and thickness. *Tectonics*, *31*(5).
Martín-Parra, L. M., Bellido, F., Rodríguez-Fernández, L. R., Suárez, A., & Zamora, G. (2016). *Mapa geológico de España E. 1:50.000, Hoja n° 181 (Esterri de Aneu), 2ª serie MAGNA*. Instituto Geológico y Minero de España.
Martínez-Peña, M. B., & Casas-Sainz, A. M. (2003). Cretaceous-tertiary tectonic inversion of the Cotiella Basin (southern Pyrenees, Spain). *International Journal of Earth Sciences*, *92*(1), 99–113. https://doi.org/10.1007/s00531-002-0283-x
Matte, P. (1969). Le probleme du passage de la schistosité horizontala la schistosité verticale dans la dôme de la Garonne (Paléozoique des Pyrénées Centrales). *Comptes Rendus de l'Académie des Sciences*, *268*, 1841–1844.
Mencos, J., Carrera, N., & Muñoz, J. A. (2015). Influence of rift basin geometry on the subsequent postrift sedimentation and basin inversion: The Organyà Basin and the Bóixols thrust sheet (south central Pyrenees). *Tectonics*, *34*, 1452–1474. https://doi.org/10.1002/2014tc003692
Mey, P. H. W., Nagtegaal, P. J. C., Roberti, K. J., & Hartevelt, J. J. A. (1968). Lithostratigraphic subdivision of post-Hercynian deposits in the south-central Pyrenees, Spain. *Leidse Geologische Mededelingen*, *41*(1), 221–228.
Moritz, H. (1980). Geodetic reference system 1980. *Bulletin Geodesique*, *54*(3), 395–405. https://doi.org/10.1007/bf02521480
Muñoz, J. A. (1992). Evolution of a continental collision belt: ECORS-pyrenees crustal balanced cross-section. In M. Clay (Ed.), *Thrust tectonics* (pp. 247–254). Chapman & Hall.
Muñoz, J. A. (2002). Alpine tectonics I: The Alpine system North of the betic Cordillera. In W. Gibbons, & T. Moreno (Eds.), *Tectonic setting; the Pyrenees geology of Spain* (pp. 370–385). Geological Society.
Muñoz, J. A. (2019). Alpine orogeny: Deformation and structure in the northern Iberian margin (Pyrenees sl). In *The geology of Iberia: A Geodynamic approach* (pp. 433–451). Springer.

Muñoz, J. A., Beamud, E., Fernández, O., Arbués, P., Dinarès-Turell, J., & Poblet, J. (2013). The Ainsa fold and thrust oblique zone of the Central Pyrenees: Kinematics of a curved contractional system from paleomagnetic and structural data. *Tectonics*, *32*, 1142–1175. https://doi.org/10.1002/tect.20070

Muñoz, J. A., Carrera, N., Mencos, J., Beamud, B., Perea, H., Arbués, P., et al. (2009). *Mapa geològic de Catalunya escala 1:25000*. Institut Geològic de Catalunya / Institut Cartogràfic de Catalunya. 252-1-2 (65-22).Full de Tremp.

Muñoz, J. A., Carrera, N., Mencos, J., Beamud, B., Perea, H., Arbués, P., et al. (2010). *Mapa Geològic de CatalunyaEscala: 25000* (Vol. 1). Institut Geològic de Catalunya. Aramunt 252-2-2 (66-22).

Muñoz, J. A., Mencos, J., Carrera, N., Gratacós, O., Ferrer, O., & Fernández, O. (2018). The structure of the south-central-Pyrenean fold and thrust belt as constrained by subsurface data. *Geológica Acta*, *16*(4), 439–460. https://doi.org/10.1344/GeologicaActa2018.16.4.7

Nagy, D. (1969). The gravitational attraction of a right rectangular prism. *Geophysics*, *31*(2), 362–371.

Nijman, W., & Nio, S. D. (1976). *The Eocene Montañana Delta: Tremp-Graus basin, Provinces of Lérida and Huesca, southern pyrenee, N. Spain*. Vakgroep Sedimentologie.

Padel, M., Clausen, S., Álvaro, J. J., & Casas, J. M. (2018). Review of the Ediacaran-lower Ordovician (pre-Sardic) stratigraphic framework of the eastern Pyrenees, southwestern Europe. *Geológica Acta*, *16*(4), 339–355.

Pallars-Jussà (2007). *Mapa geològic comarcal de Catalunya 1:50000*. Institut Cartogràfic i Geològic de Catalunya. (ICGC), used under the license CC BY 4.0".

Pallars-Sobirà (2007). *Mapa geològic comarcal de Catalunya 1:50000*. Institut Cartogràfic i Geològic de Catalunya. (ICGC), used under the license CC BY 4.0".

Parish, M. (1984). A structural interpretation of a section of the Gavarnie nappe and its implications for Pyrenean geology. *Journal of Structural Geology*, *6*(3), 247–255. https://doi.org/10.1016/0191-8141(84)90049-x

Pedrera, A., García-Senz, J., Ayala, C., Ruiz-Constán, A., Rodríguez-Fernández, L. R., Robador, A., & González-Menéndez, L. (2017). Reconstruction of the exhumed mantle across the North Iberian Margin by crustal-scale 3-D gravity inversion and geological cross section. *Tectonics*, *413*, 150–154. https://doi.org/10.1002/2017tc004716

Poblet, J. (1991). *Estructura herciniana i alpina del Vessant sud de la zona Axial del Pirineu Central*. Unpublished PhD Thesis, Univ. of Barcelona, 604 pp.

Puigdefàbregas, C., & Souquet, P. (1986). Tecto-sedimentary cycles and depositional sequences of the Mesozoic and tertiary from the Pyrenees. *Tectonophysics*, *129*(1–4), 173–203.

Ribargorça, A. (2007). *Mapa geològic comarcal de Catalunya 1:50000*. Institut Cartogràfic i Geològic de Catalunya. (ICGC), used under the license CC BY 4.0".

Ríos-Aragües, L. M., Galera-Fernández, J. M., Barettino, D., & Charlet, J. M. (2002). *Mapa geológico de España E. 1:50.000, Hoja n° 180 (Benasque), 2ª serie MAGNA*. Instituto Geológico y Minero de España.

Rivero Marginedas, L. (1994). Estudio Gravimétrico del Pirineo Oriental. *Acta Geologica Hispanica*, *29*(1), 81–83.

Rivero, L., Pinto, V., & Casas, A. (2002). Moho depth structure of the eastern part of the Pyrenean belt derived from gravity data. *Journal of Geodynamics*, *33*(3), 315–332. https://doi.org/10.1016/s0264-3707(01)00073-4

Roest, W. R., & Srivastava, S. P. (1991). Kinematics of the plate boundaries between Eurasia, Iberia, and Africa in the north Atlantic from the late Cretaceous to the present. *Geology*, *19*(6), 613–616. https://doi.org/10.1130/0091-7613(1991)019<0613:kotpbb>2.3.co;2

Rosell, J. (1994). *Mapa geológico de España E. 1:50.000, Hoja n° 252 (Tremp), 2ª serie MAGNA*. Instituto Geológico y Minero de España.

Rosenbaum, G., Lister, G. S., & Duboz, C. (2002). Relative motions of Africa, Iberia and Europe during Alpine orogeny. *Tectonophysics*, *359*(1-2), 117–129. https://doi.org/10.1016/S0040-1951(02)00442-0

Saltus, W. R., & Blakely, R. (2011). Unique geologic insights from "non-unique" gravity and magnetic interpretationGSA. *Today's Office*, *21*(12), 4–10. https://doi.org/10.1130/G136A.1

Sandwell, D. T., Gille, S. T., & Smith, W. H. F. (2002). *Bathymetry from Space: Oceanography, Geophysics, and Climate* (p. 24). Geoscience Professional Services.

Santolaria, P., Ayala, C., Pueyo, E. L., Rubio, F. M., Soto, R., Calvín, P., et al. (2020). Structural and geophysical characterization of the western termination of the South Pyrenean triangle zone. *Tectonics*, *39*(8). https://doi.org/10.1029/2019tc005891

Santolaria, P., Casas, A., Casas-Sainz, A. M., & Soto, R. (2016). Gravimetric modelling to assess salt tectonics in the western end of the south Pyrenean central unit. *Journal of the Geological Society*, *174*(2), 269–288. https://doi.org/10.1144/jgs2016-027

Sanz-López, J., & Palau, J. (2013). *Mapa geológico de España E. 1:50.000, Hoja n° 149 (Isil), 2ª serie MAGNA*. Instituto Geológico y Minero de España.

Sarsar-Naouali, B. S., Inoubli, M. H., Amiri, A., Chaqui, A., & Hamdi, I. (2011). Subsurface geology of the Ariana region (Diapir Zone, northern Tunisia) by means of gravity analysis. *Geophysical Prospecting*, *59*, 983–997. https://doi.org/10.1111/j.1365-2478.2011.01004.x

Saspiturry, N., Razin, P., Baudin, T., Serrano, O., Issautier, B., Lasseur, E., et al. (2019). Symmetry vs. asymmetry of a hyper-thinned rift: Example of the Mauléon basin (western Pyrenees, France). *Marine and Petroleum Geology*, *104*, 86–105. https://doi.org/10.1016/j.marpetgeo.2019.03.031

Saura, E. (2004). *Anàlisi estructural de la zona de les Nogueres Pirineus Centrals*. PhD Thesis (p. 355). Universitat Autònoma de Barcelona.

Saura, E., Ardèvol, L., Teixell, A., & Vergés, J. (2016). Rising and falling diapirs, shifting depocenters, and flap overturning in the Cretaceous Sopeira and Sant Gervàs subbasins (Ribagorça Basin, southern Pyrenees). *Tectonics*, *35*, 638–662. https://doi.org/10.1002/2015TC004001

Saura, E., & Teixell, A. (2006). Inversion of small basins: Effects on structural variations at the leading edge of the axial zone antiformal stack (southern Pyrenees, Spain). *Journal of Structural Geology*, *28*(11), 1909–1920. https://doi.org/10.1016/j.jsg.2006.06.005

Schön, J. (2011). *Chapter 4 – densityPhysical properties of rocks: A workbook*. (Vol. 8, pp. 97–105). Elsevier.

Seguret, M. (1972). Étude tectonique des nappes et séries décollées de la partie centrale du versant sud des Pyrénées. *Pub. Estela, Ser geol. struct.*, *2*, 1–155.

Simó, A. (1986). Carbonate platform depositional sequences, Upper Cretaceous, south-central Pyrenees (Spain). *Tectonophysics*, *129*(1–4), 205–231.

Simó, A. (2004). El Cretácico superior de la Unidad Surpirenaica central. In J. A. Vera (Ed.), *Geología de España* (pp. 296–299). Sociedad Geológica de España-Instituto Geológico y Minero de España.

Solé, J., Soler, A., Palau, J., Espiuola, M. P., & Delgado, J. (1997). *Geocronología K/Ar de los Skarn Mineralizados en As-Au y de las alteraciones intragraníticas asociadas en el Hercínico de los Pirineos centrales* (pp. 77–78). Boletín de la Sociedad Española de Mineralogía 20A.

Soler, A. (1990). Gelogia i metalogenia de la terminció sud del granit d'Andorra (Pirineu Central). Tesis doctoral. Universitat de Barcelona, 886.

Soler, D., Teixell, A., García-Sansegundo, J. (1998). Amortissement latéral du chevauchement de Gavarnie et sa relation avec les unités sud-pyrénéenes. *Comptes Rendus Acad Sci Paris*, *327*, 699–704.

Soto, R., Storti, F., & Casas-Sainz, A. M. (2006). Impact of backstop thickness lateral variations on the tectonic architecture of orogens: Insights from sandbox analogue modeling and application to the Pyrenees. *Tectonics*, *25*(2). https://doi.org/10.1029/2004tc001693

Storti, F., Soto-Marín, R., Rossetti, F., & Sainz, A. C. (2007). Evolution of experimental thrust wedges accreted from along-strike tapered, silicone-floored multilayers. *Journal of the Geological Society*, *164*(1), 73–85. https://doi.org/10.1144/0016-76492005-186

Sussman, A. J., Butler, R. F., Dinarès-Turell, J., & Vergés, J. (2004). Vertical-axis rotation of a foreland fold and implications for orogenic curvature: An example from the southern Pyrenees, Spain. *Earth and Planetary Science Letters*, *218*(3–4), 435–449. https://doi.org/10.1016/s0012-821x(03)00644-7

Talwani, M., Worzel, J. L., & Landisman, M. (1959). Rapid gravity computations for two-dimensional bodies with application to the Mendocino submarine fracture zone. *Journal of Geophysical Research*, *64*(1), 49–59. https://doi.org/10.1029/jz064i001p00049

Teixell, A. (1996). The Ansó transect of the southern Pyrenees: Basement and cover thrust geometries. *Journal of the Geological Society*, *153*(2), 301–310. https://doi.org/10.1144/gsjgs.153.2.0301

Teixell, A. (1998). Crustal structure and orogenic material budget in the west central Pyrenees. *Tectonics*, *17*(3), 395–406. https://doi.org/10.1029/98tc00561

Teixell, A., Labaume, P., Ayarza, P., Espurt, N., Saint Blanquat, M., & Lababrielle, Y. (2018). Crustal structure and evolution of the pyrenean-Cantabrian belt: A review and new interpretations from recent concepts and data. *Tectonophysics*, *724–725*, 146–170. https://doi.org/10.1016/j.tecto.2018.01.009

Teixell, A., & Muñoz, J. A. (2000). Evolución tectono-sedimentaria del Pirineo meridional durante el Terciario: Una síntesis basada en la transversal del río Noguera Ribagorçana. *Revista de la Sociedad Geologica de Espana*, *13*, 251–264.

Ten Brink, U. S., Ben-Avraham, Z., Bell, R. E., Hassouneh, M., Coleman, D. F., Andreasen, G., et al. (1993). Structure of the Dead Sea pull-apart basin from gravity analyses. *Journal of Geophysical Research*, *98*(B12), 21877–21894. https://doi.org/10.1029/93jb02025

Terrinha, P., Pueyo, E. L., Aranguren, A., Kullberg, J. C., Kullberg, M. C., Casas-Sainz, A., & do Rosário Azevedo, M. (2018). Gravimetric and magnetic fabric study of the Sintra igneous complex: Laccolith-plug emplacement in the western Iberian passive margin. *International Journal of Earth Sciences*, *107*(5), 1807–1833. https://doi.org/10.1007/s00531-017-1573-7

Torné, M., De Cabissole, B., Bayer, R., Casas, A., Daignières, M., & Rivero, A. (1989). Gravity constraints on the deep structure of the Pyrenean belt along the ECORS profile. *Tectonophysics*, *165*(1–4), 105–116.

Torné, M., Fernàndez, M., Vergés, J., Ayala, C., Salas, M. C., Jimenez-Munt, Y., et al. (2015). Crust and mantle lithospheric structure of the Iberian Peninsula deduced from potential field modeling and thermal analysis. *Tectonophysics*, *663*, 419–433.

UNE-EN (1936). *2007, Métodos de ensayo para piedra natural. Determinación de la densidad real y aparente y de la porosidad abierta y total*. UNE.org.

Vacher, P., & Souriau, A. (2001). A three-dimensional model of the Pyrenean deep structure based on gravity modelling, seismic images and petrological constraints. *Geophysical Journal International*, *145*, 460–470. https://doi.org/10.1046/j.0956-540x.2001.01393.x

Vergés, J. (1993). *Estudi geològic del vessant sud del Pirineu oriental i central. Evolució cinemàtica en 3D*. PhD Thesis (p. 192). Univ. de Barcelona.

Vergés, J., Millán, H., Roca, E., Muñoz, J. A., Marzo, M., Cirés, J., et al. (1995). Eastern Pyrenees and related foreland basins: Pre-, syn-and post-collisional crustal-scale cross-sections. *Marine and Petroleum Geology*, *12*(8), 903–915.

Verges, J., & Munoz, J. A. (1990). Thrust sequence in the southern central Pyrenees. *Bulletin de la Societe Geologique de France*, *6*(2), 265–271. https://doi.org/10.2113/gssgfbull.vi.2.265

Vigneresse, J. L., & Clemens, J. D. (2000). Granitic magma ascent and emplacement: Neither diapirism nor neutral buoyancy. In B. Vendeville, Y. Mart, & J. L. Vigneresse (Eds.), *Slate, Shale and Igneous Diapirs in and Around Europe* (Vol. 174, pp. 1–19). Geol. Soc. London, Spec. Publication. https://doi.org/10.1144/gsl.sp.1999.174.01.01

Wang, Y., Chevrot, S., Monteiller, V., Komatitsch, D., Mouthereau, F., Manatschal, G., et al. (2016). The deep roots of the western Pyrenees revealed by full waveform inversion of teleseismic P waves. *Geology*, *44*(6), 475–478. https://doi.org/10.1130/g37812.1

Williams, G. D. (1985). Thrust tectonics in the south central Pyrenees. *Journal of Structural Geology*, *7*(1), 11–17. https://doi.org/10.1016/0191-8141(85)90111-7

Won, I. J., & Bevis, M. (1987). Computing the gravitational and magnetic anomalies due to a polygon: Algorithms and Fortran subroutines. *Geophysics*, *52*(2), 232–238. https://doi.org/10.1190/1.1442298

Zwart, H. J. (1979). The geology of the central Pyrenees. *Leidse Geologische Mededelingen*, *50*, 1–74.